THE ASTROPHYSICAL JOURNAL, 433:583–601, 1994 October 1

ABUNDANCE GRADIENTS IN COOLING FLOW CLUSTERS: *GINGA* LARGE AREA COUNTERS AND *EINSTEIN* SOLID STATE SPECTROMETER SPECTRA OF A496, A1795, A2142, AND A2199

RAYMOND E. WHITE III,[1] C. S. R. DAY,[2,3] ISAMU HATSUKADE,[4] AND JOHN P. HUGHES[5]
Received 1994 March 9; accepted 1994 April 11

ABSTRACT

We analyze the *Ginga* LAC and *Einstein* SSS spectra of four cooling flow clusters, A496, A1795, A2142, and A2199, each of which shows firm evidence of a relatively cool component. The inclusion of such cool spectral components in joint fits of SSS and LAC data leads to somewhat higher global temperatures than are derived from the high-energy LAC data alone. We find little evidence of cool emission outside the SSS field of view. Metal abundances appear to be centrally enhanced in all four clusters, with varying degrees of model dependence and statistical significance: the evidence is statistically strongest for A496 and A2142, somewhat weaker for A2199 and weakest for A1795. We also explore the model dependence in the amount of cold, X-ray–absorbing matter discovered in these clusters by White et al.

Subject headings: cooling flows — galaxies: abundances — galaxies: clusters of — X-rays: galaxies

1. INTRODUCTION

Some of the most accurate temperatures and iron abundances available for the hot gas in many galaxy clusters have been obtained from X-ray spectra taken with the Large Area Counters (LACs) on the *Ginga* satellite (Takano et al. 1989; Hatsukade 1989; McHardy et al. 1990; Koyama, Takano, & Tawara 1991; Day et al. 1991; Arnaud et al. 1991, 1992; Birkinshaw, Hughes, & Arnaud 1991; Ikebe et al. 1992; Allen et al. 1992; Johnstone et al. 1992; Hughes & Tanaka 1992; Hughes et al. 1993). However, with an effective lower energy limit of ~ 1 keV, the LAC was not very sensitive to the spectral signature of cooling flows which occur in the centers of many clusters. In contrast, the lower-energy *Einstein Observatory* Solid State Spectrometer (SSS) and Focal Plane Crystal Spectrometer (FPCS) were particularly sensitive to emission from cooling flows passing through temperatures $kT \lesssim 1$ keV (Mushotzky & Szymkowiak 1988; Canizares, Markert, & Donahue 1988). Recent reanalysis of cluster SSS spectra has also revealed large quantities of relatively cold, X-ray–absorbing gas in many cooling flow clusters, quantities well in excess of the Galactic column of cold material in their lines of sight (White et al. 1991, hereafter WFJMA). This intrinsic absorption is attributed to the accumulation of cooling flow condensates and may account for much of the total material likely to have been accreted during the lives of the cooling flows (WFJMA). Wang & Stocke (1993) also found evidence of absorption in *Einstein* IPC spectra of distant clusters. Furthermore, spatially resolved *ROSAT* PSPC spectra of the copious cooling flow cluster A478 confirm the SSS evidence for an absorption component and also show that it is indeed confined to the cooling flow (Allen et al. 1993).

While many clusters have had analyses of their SSS or LAC spectra published, only one cluster, A478, has had its LAC and SSS data analyzed together, although the spectral models were not fit simultaneously (Johnstone et al. 1992). Joint analyses of SSS and LAC spectra are particularly informative because their different passbands provide complementary constraints on spectral models, particularly when their differing fields of view are taken into account: the SSS had a circular field of view with a 6′ diameter (flat top), while the LACs had a much larger, elliptical field of view, $1° \times 2°$ (FWHM). The complementary nature of these data is illustrated by considering a cluster which is largely isothermal except for a central cooling flow which is cooling from the same temperature as the exterior cluster gas. If such a cluster were nearby, a centered SSS spectrum would be dominated by the cooling flow emission, while the LAC spectrum would include emission from the entire cluster. The cooling flow spectrum would be determined in part by its initial temperature, but this temperature would tend to be underestimated by an analysis of the soft SSS spectrum alone. The LAC spectrum, in turn, would provide an accurate global temperature and abundance, but would not be able to constrain the properties of the cooling flow (accretion rate, abundances, internal absorption) very well because much of the cooling flow emission and the effects of internal absorption would be most evident at energies lower than the LAC passband.

The power of joint spectral analysis is best realized by fitting the complementary spectra simultaneously. Hughes & Tanaka (1992) simultaneously analyzed the *Einstein* IPC and *Ginga* LAC spectra of A665 and were able to constrain its temperature distribution. These authors found this could not have been achieved by analyzing the data sets separately. Moreover, simultaneous fitting allows more accurate assessment of the parameter uncertainties, since all the relevant model fitting parameters can co-vary in the course of error analysis.

Inspection of the isothermal fits to LAC spectra in Hatsukade (1989) reveals persistent positive residuals below ~ 2 keV in several clusters known to have cooling flows. Whether these positive soft residuals are due to central cooling flows or, say, to cool emission in the outer parts of clusters may be distinguished by a joint analysis of the SSS and LAC spectra. If the

[1] Department of Physics and Astronomy, University of Alabama, Box 870324, Tuscaloosa, AL 35487-0324.
[2] Laboratory of High Energy Astrophysics, NASA/GSFC, Greenbelt, MD 20771.
[3] USRA Research Associate.
[4] Department of Electronic Engineering, Miyazaki University, 1-1 Gakuen Kibanadai, Nishi, Miyazaki, 889-21, Japan.
[5] Harvard-Smithsonian Center for Astrophysics, 60 Garden Street, Cambridge, MA 02138.

cool emission is fully accounted for within the smaller SSS field of view, the cool emission seen in the LAC spectra is not likely to come from cluster exteriors. The differing fields of view can also be exploited to determine whether there are gradients in abundances or cool X-ray absorbing material.

In this paper, we investigate these possibilities with a joint analysis of the LAC and SSS X-ray spectra for four clusters, A496, A1795, A2142, and A2199. In § 2 we describe how the cluster X-ray spectral data were reduced. We analyze the four individual clusters in § 3, in order of Abell number (which are in right ascension order). A2199 and A496 have the highest quality data, followed by A1795, while A2142, the most distant cluster of the four, has the poorest statistics. We summarize and further discuss our results in § 4. Imaging data will be incorporated in later studies of individual clusters.

2. DATA REDUCTION

2.1. *Ginga LAC spectra*

The *Ginga* observations presented here of A496, A1795, and A2142 have been analyzed before by Hatsukade (1989), who primarily investigated isothermal models. For these clusters, we use a similar set of reduced *Ginga* data as Hatsukade (1989). Analysis of the *Ginga* observations of A2199 has not been previously published.

The eight LACs on *Ginga* covered the energy range 1–37 keV with 48 channels and an energy resolution of 18% at 6 keV. The (unimaged) field of view was 1° × 2° FWHM and the combined geometric collecting area was 4000 cm^2. Descriptions of *Ginga* and the LACs can be found in Makino et al. (1987) and Turner et al. (1989), respectively. The data for A496, A1795, and A2142 are collected from the top and middle of the three LAC layers, while the data for A2199 are from the top layer alone. A log of the *Ginga* observations is given in Table 1. The *Ginga* observations of these four clusters yielded spectra integrated over the entire cluster and their immediate surroundings with high signal-to-noise but modest spectral resolution.

Of primary concern when reducing *Ginga* data from moderate to faint sources is the proper subtraction of the background, both X-ray and non–X-ray. We adopt the most straightforward way of removing the background: subtracting an observation of a nearby blank field taken on an adjacent day. By observing a nearby field, the dependence of the diffuse X-ray background on sky position is accounted for, while observing on an adjacent day ensures that the geomagnetic conditions of the background closely match those of the cluster. In addition, we discard data collected from the five (of 15) satellite orbits per day which passed through the South Atlantic Anomaly, thereby incurring a high background.

Each spectrum was associated with a response matrix tailored to the gain state of the LAC at the time of the observation. To guard against misinterpreting subtle spectral features caused by residual uncertainties in the response matrix, we followed the standard practice of adding systematic errors of 1% to the spectral (PHA) data. We ignored PHA channels 1–2, which do not contain valid data, and high-energy channels where the sensitivity falls off, leaving an energy range of 1.2–17.4 keV. A few channels in some of the cluster spectra were rebinned to improve statistics.

2.2. *Einstein SSS spectra*

We extracted the SSS spectra of the four clusters from the HEASARC data base (see Table 1 for the observation log). Ice accumulated on the spectrometer entrance window in a time variable manner (through a series of frost and defrost cycles), causing variable absorption of soft X-rays, so each spectral data file requires its own response matrix. The latest models of ice buildup were incorporated into the response matrix gener-

TABLE 1

SPECTRAL DATA LOG

cluster	det	seq #	time (yr.day)	expos (sec)	count rate	ice	Δ ice	RA (1950)	Dec (1950)	comment
A496	SSS	1433	79.221	6144	0.64	0.75	0.11	4 31 18	-13 22 05	hi Δice
	"	"	79.222	5652	0.63	1.00	0.02	4 31 18	-13 22 05	
	"	"	79.223	7372	0.65	1.02	0.03	4 31 18	-13 22 05	
	LAC		88.288	12618	32.9	...	...	4 31	-13 21	
A1795	SSS	1442	79.018	5816	0.59	2.61	0.01	13 46 34	+26 50 24	hi ice
	"	"	79.195	1228	0.77	0.44	0.26	13 46 33	+26 50 36	hi Δice
	"	"	79.196	4587	0.68	0.79	0.38	13 46 33	+26 50 36	hi Δice
	"	"	79.197	7864	0.72	1.27	0.02	13 46 33	+26 50 36	
	"	"	79.198	5242	0.62	1.35	0.01	13 46 33	+26 50 36	
	"	"	79.199	6062	0.61	1.39	0.03	13 46 33	+26 50 36	
	LAC		88.174	10493	47.1	...	...	13 46	+26 51	
A2142	SSS	1431	79.232	5898	0.74	0.81	0.03	15 56 15	+27 22 10	
	"	"	79.233	15155	0.73	0.86	0.08	15 56 15	+27 22 10	
	"	"	79.234	5160	0.70	0.94	0.02	15 56 15	+27 22 10	
	LAC		88.222	8827	40.0	...	...	15 56	+27 22	
A2199	SSS	1440	79.209	8929	0.77	1.02	0.02	16 26 55	+39 39 36	
	"	"	79.231	5652	0.91	0.67	0.02	16 26 55	+39 39 36	
	"	"	79.232	10240	0.96	0.70	0.03	16 26 55	+39 39 36	
	LAC		90.068	22024	38.4	...	...	16 26	+39 39	

NOTES.—det, detector; seq #, sequence number of observation; time, year and day of observation; expos, exposure time; count rate in counts s^{-1}; ice, ice parameter; Δice, change in ice parameter during observation; RA and Dec, pointing position; comment: reason spectrum rejected from consideration: Δice/ice > 10% or ice relatively high compared to others.

ation and are advertised to work best for spectra in which the ice parameter changes by less than 10% during the integration. The new ice models obviate the inclusion of the previously recommended 2% systematic errors (Christian et al. 1992). The statistical errors are far larger than any residual systematic errors. PHA channels 1 and 86–94 were ignored, leaving an approximate energy range of 0.5–4.5 keV, which overlaps the low-energy *Ginga* LAC spectral coverage. Some channels were rebinned to improve statistics. To analyze the SSS spectra, we followed the detailed prescription given by Drake, Arnaud, & White (1992), which describes how to subtract the two SSS background components (see Szymkowiak 1986 and WFJMA).

3. DATA ANALYSIS

The *Ginga* LAC spectra of three of these clusters are among the 11 analyzed previously by Hatsukade (1989), who fitted a variety of spectral models: thermal bremsstrahlung, bremsstrahlung plus one and two emission lines (due to iron Kα and Kβ), and collisional ionization equilibrium (CIE) models based on the emissivity calculations of Masai (1984). An additional power-law component was considered for two clusters which are not in the current subset.

The *Einstein* SSS spectra of these clusters were previously analyzed by Mushotzky (1984), Mushotzky & Szymkowiak (1988), and WFJMA. In reanalyzing nearly all the clusters in the SSS database, WFJMA discovered the need for considerable amounts of intrinsic absorption in most of the clusters with cooling flows. As mentioned above, this intrinsic absorption component tends to be well in excess of the Galactic column, and was attributed to the accumulation of cooling flow condensates over the lives of the cooling flows.

We used the XSPEC (version 8.33) software package to individually and simultaneously analyze the SSS and LAC spectra for each cluster. We fitted a variety of spectral models, including single- and dual-temperature thermal models, and thermal plus cooling flow models, among others. In models with two emission components, we also allowed the abundances of the two components to vary independently. The results of the model fits are listed in Tables 2–5, the entries of which are described in the notes to Table 2; for brevity we will refer to specific model results by table and line number: e.g., T2.1 refers to line 1 of Table 2. The results of these fits are now described for each cluster in turn.

3.1. *Abell 496*

Abell 496 is a Bautz-Morgan Type I cluster with a central cD. At a redshift $z = 0.0320$, the luminosity distance to A496 is 193 h_{50}^{-1} Mpc and $1' = 53\ h_{50}^{-1}$ kpc (where h_{50} is the Hubble constant in units of 50 km s^{-1} Mpc^{-1}, and we take $q_0 = \frac{1}{2}$, so the angular diameter distance is 182 h_{50}^{-1} Mpc). The LAC field of view (FWHM) encompasses $3.2 \times 6.4\ h_{50}^{-1}$ Mpc at this distance, while the SSS field of view has a 318 h_{50}^{-1} kpc diameter. The cluster appears dynamically relaxed, since it does not have much velocity or spatial substructure (Zabludoff, Huchra, & Geller 1990, hereafter ZHG) and its IPC X-ray images have smooth isophotes in the central region. The IPC images show no serendipitous sources with sufficient flux to be significant compared to that of the cluster. The nominal center of the SSS field of view is 0.'24 from the IPC X-ray peak, while the nominal center of the larger LAC field of view is 4.'6 away from the IPC X-ray peak.

The presence of a cooling flow in A496 was first posited by Heckman (1981) on the basis of its central Hα emission, thought to be due to cooling flow condensates cooling through 10^4 K. More recent optical observations show extended emission (Cowie et al. 1983, hereafter CHJY). Nulsen et al. (1982) found a soft X-ray component in the *Einstein* SSS spectra for this cluster and estimated a cooling accretion rate of $\sim 200\ M_\odot$ yr^{-1}. Subsequent analysis of SSS spectra by Mushotzky (1984) and Mushotzky & Szymkowiak (1988) indicated an accretion rate of 200–400 $M_\odot$ yr^{-1}, while Canizares et al. (1988) derived upper limits of 200 and 310 $M_\odot$ yr^{-1} from individual X-ray lines in FPCS spectra. Further imaging analyses of IPC data by Arnaud & Fabian (1987) and Thomas, Fabian, & Nulsen (1987) derived a total accretion rate of $\sim$100–120 $M_\odot$ yr^{-1} and a cooling radius of $\sim$3.'0–3.'4. The larger of these cooling radius estimates extends 0.'4 beyond the SSS field of view. However, in both of these imaging analyses, the age of the cooling flow was assumed to be 2×10^{10} yr. Depending upon the cooling time criterion adopted, this may lead to an overestimate of the cooling radius by as much as a factor of $\gtrsim 2$ if the true age is $\lesssim 10^{10}$ yr, given the observed density profile. Thus, the bulk of the cooling flow emission may be within the SSS field of view, but we test this below.

3.1.1. *Separate LAC and SSS Spectral Fits*

We fitted a Raymond-Smith (hereafter denoted RS) isothermal model for the X-ray emission from an optically thin hot plasma in collisional ionization equilibrium (Raymond & Smith 1977) to the LAC data for comparison with the results of Hatsukade (1989). In XSPEC, the cosmic abundance of iron (by number) relative to hydrogen is -4.5 dex, while Hatsukade (1989) adopted a value of -4.4 dex (Allen 1976). Our abundance determinations (which are driven mostly by iron) will then be ~ 1.26 times larger than Hatsukade's for the same iron fraction. For this comparison we adopted the same Galactic line-of-sight hydrogen column density as Hatsukade (1989): $N_H = 5 \times 10^{20}$ cm^{-2} (N_H is used to parameterize the soft X-ray absorption due to cool intervening Galactic material—see Morrison & McCammon 1983). Although the best fit is not good (the reduced χ^2 per degree of freedom $\chi^2_\nu = 2.21$ for $\nu = 19$ degrees of freedom; see line 1 of Table 2, denoted T2.1), we found the temperature and abundance to be well determined, with $kT = 3.97$ (3.91–4.04) keV and $A = 0.48$ (0.43–0.53), where A is the heavy element abundance relative to the cosmic value (A is assumed to be the same for all elements) and the values in parentheses are 90% confidence intervals (see Table 2, where the 90% confidence limits vertically bracket the best-fit values). Using Masai emissivities, Hatsukade (1989) found a slightly smaller temperature, $kT = 3.91$ (3.84–3.97) keV, and a slightly larger iron abundance, $A = 0.53$ (0.48–0.58) (adjusting upward a factor of 1.26), which are nonetheless within the 90% confidence intervals of the present values. If the column density of hydrogen is allowed to vary freely, it is not well determined. Zero column provides the smallest χ^2, reducing χ^2 by 10.6 while reducing the number of degrees of freedom ν by one. That the previous model (see T2.1) has larger χ^2 is due to the fact that there is excess emission compared to the model at the lowest energies, which becomes even more obvious when the minimum expected absorption (due to the Galaxy) is taken into account in the model. This excess emission is likely due to a relatively cool component analyzed further below.

We also analyzed the two SSS spectra (of three total) for which the ice varied by less than 10% in the course of the

TABLE 2

A496 MODEL-FIT PARAMETERS

	model - inst	kT	A	N_H	LAC norm	SSS norm	cool kT	cool A	cool N_H	cool norm	χ^2	ν	PHA	χ_ν^2	prob	comment
		4.04	0.53		10.16											
(1)	a rs - LAC	3.97	0.48	5.0*	10.01						42.0	19	22	2.21	1.8-3	1T,1A
		3.91	0.43		9.85											
		4.34	2.28	14.6		3.32										
(2)	a rs - SSS	3.68	1.50	12.0		2.89					118.8	148	152	0.80	0.97	1T,1A,1H
		3.08	0.94	9.9		2.51										
(3)	a rs	3.90	0.51	10.6	10.16	3.53					203.3	169	174	1.20	0.037	1T,1A,1H
(4)	a(z(rs)+rs)	4.34	0.53	4.5*	8.47	1.83	1.60	0.53=	35.4	2.15	163.3	167	174	0.98	0.50	2T,1A,1.5H
		4.41	0.53		9.12	2.38	2.01	>5.00	55.8	1.57						
(5)	a(z(rs)+rs)	4.30	0.47	4.5*	8.79	2.13	1.64	2.63	40.1	0.76	153.6	166	174	0.93	0.75	2T,2A,1.5H
		4.19	0.42		8.29	1.70	1.39	1.01	24.9	0.26						
(6)	a(rs+rs)	4.06	0.47	11.9	9.70	2.87	1.51	9.97		0.10	157.5	166	174	0.95	0.67	2T,2A,1H
		4.29	0.37		8.91	2.04		>9.00	45.6	188						
(7)	a(z(cf)+rs)	4.20	0.25	4.5*	8.57	1.71	4.20=	3.79	38.5	154	151.7	167	174	0.91	0.80	1T,2A,1.5H
		4.12	0.16		8.03	1.27		1.58	32.3	127						
(8)	a(z(cf)+rs)	4.20	0.51	4.5*	7.68	1.16	4.20=	0.51=	31.3	194	168.6	168	174	1.00	0.47	1T,1A,1.5H
(9)	a(cf+rs)	4.13	0.29	16.8	9.45	2.46	4.13	4.53		91	192.3	167	174	1.15	0.087	1T,2A,1H

NOTES.—Models are fitted jointly to LAC and SSS unless otherwise noted under "inst."

Model components:

a, Wisconsin absorption model (Morrison & McCammon 1983); z, redshifted intrinsic absorption; rs, Raymond-Smith thermal model; cf, cooling flow model of Mushotzky & Szymkowiak (1988), with slope fixed at 0; kT, temperature in keV; A, abundance relative to solar; N_H, line-of-sight column density of neutral hydrogen $\times 10^{20}$ cm^{-2}; norm, normalization: Raymond-Smith normalization in 10^{12} cm^{-5}; cooling flow normalization in $M_\odot$/yr^{-1}; cool norm is normalization of component taken to be common to LAC and SSS fields of view; ν, degrees of freedom in spectral fit; PHA, number of data channels fit; χ_ν^2, χ^2 per degree of freedom; prob, probability that model can produce χ^2 greater than it does; comment, code for number of independent temperatures T, abundances A and column densities H; (1.5H ⇒ one free (intrinsic) column plus one fixed Galactic column).

"*" ⇒ fixed parameter.

" = " ⇒ tied parameter.

1994ApJ...433..583W

TABLE 3

A1795 MODEL FIT PARAMETERS

	model - inst	*kT*	*A*	N_H	LAC norm	SSS norm	cool *kT*	cool *A*	cool N_H	cool norm	χ^2	ν	PHA	χ_ν^2	prob	comment
		5.69	0.48		8.24											
(1)	a rs - LAC	5.57	0.43	1.7*	8.12						21.8	19	22	1.15	0.29	1T,1A
		5.45	0.38		8.00											
		4.14	0.24	5.2		5.52										
(2)	a rs - SSS	3.67	0.06	3.7		5.16					241.5	225	229	1.07	0.22	1T,1A,1H
		3.26	0.00	2.2		4.80										
		5.67	0.48	0.8	8.22	4.45										
(3)	a rs	5.57	0.43	0.0	8.10	4.36					283.9	246	251	1.15	0.049	1T,1A,1H
		5.45	0.38	0.0	7.99	4.29										
		5.87	0.48		8.05	4.12	0.90		75.5	2.40						
(4)	a(z(rs)+rs)	5.73	0.43	1.1*	7.91	3.97	0.74	0.43=	51.5	1.24	242.4	244	251	0.99	0.52	2T,1A,1.5H
		5.59	0.38		7.76	3.82	0.58		24.0	0.65						
		6.33	0.50		6.84	2.99			11.5	533						
(5)	a(z(cf)+rs)	6.07	0.45	1.1*	6.31	2.43	6.07=	0.45=	8.9	411	252.6	245	251	1.03	0.36	1T,1A,1.5H
		5.85	0.40		5.79	1.88			5.8	290						
			0.37					0.71								
(6)	a(z(cf)+rs)	6.26	0.14	1.1*	5.58	1.73	6.26=	0.58	8.4	558	248.7	244	251	1.02	0.42	1T,2A,1.5H
			0.04					0.46								
(7)	a(cf+rs)	6.04	0.44	4.7	6.42	2.51	6.04=	0.44=		395	254.2	245	251	1.04	0.33	1T,1A,1H

See notes for Table 2.

TABLE 4

A2142 MODEL FIT PARAMETERS

	model - inst	*kT*	*A*	N_H	LAC norm	SSS norm	cool *kT*	cool *A*	cool N_H	cool norm	χ^2	ν	PHA	χ_ν^2	prob	comment
(1)	a rs - LAC	9.18 8.99 8.78	0.39 0.34 0.29	5.0*	9.02 8.89 8.78						17.8	21	24	0.85	0.66	1T,1A
(2)	a rs - SSS	9.01 7.81 6.74	3.26 1.97 1.08	9.5 8.4 7.2		3.72 3.35 2.96					234.0	248	252	0.94	0.73	1T,1A,1H
(3)	a rs	8.90	0.34	7.8	8.95	4.07					266.0	271	276	0.98	0.57	1T,1A,1H
(4)	a(z(rs)+rs)	8.94	0.20 0.00 0.00	3.8*	5.07	0.01	8.94=	0.89 0.81 0.53	4.6	3.83	259.4	269	276	0.96	0.65	1T,2A,1.5H
(5)	a(z(rs)+rs)	10.36 9.91 9.46	0.22 0.00 0.00	3.8*	8.25 7.81 6.08	3.27 2.75 1.86	6.51 5.23 4.01	>4.00 2.97 0.99	38.7 19.6 13.3	2.05 1.02 0.37	254.0	268	276	0.95	0.72	2T,2A,1.5H
(6)	a(z(rs)+rs)	9.94	0.34*	3.8*	7.69	2.79	3.94	2.35 0.97 0.39	26.7	1.25	260.3	269	276	0.97	0.64	2T,1.5A,1.5H
(7)	a(z(rs)+rs)	10.07	0.38	3.8*	7.17	2.31	5.02	0.38=	16.8	1.82	262.9	269	276	0.98	0.59	2T,1A,1.5H
(8)	a(z(cf)+rs)	9.87 9.60 9.34	0.32 0.12 0.00	3.8*	8.41 8.04 7.64	3.31 3.00 2.50	9.60=	>5.60 3.60 0.93	54.5 44.9 34.2	545 439 345	256.4	269	276	0.95	0.70	1T,2A,1.5H
(9)	a(z(cf)+rs)	9.58	0.39	3.8*	7.62	2.74	9.58=	0.39=	35.6	475	262.8	270	276	0.97	0.61	1T,1A,1.5H
(10)	a(cf+rs)	9.10	0.35	9.4	8.50	3.56	9.10=	0.35=		177	264.0	270	276	0.98	0.59	1T,1A,1H

See notes for Table 2.

1994ApJ...433..583W

TABLE 5

A2199 MODEL FIT PARAMETERS

	model - inst	*kT*	*A*	N_H	LAC norm	SSS norm	cool *kT*	cool *A*	cool N_H	cool norm	χ^2	ν	PHA	χ_ν^2	prob	comment
		4.54	0.46	1.6	11.09											
(1)	a rs - LAC	4.48	0.43	0.0	10.96						24.3	22	26	1.10	0.33	1T,1A,1H
		4.41	0.39	0.0	10.83											
		3.70	0.82	9.1		4.70										
(2)	a rs - SSS	3.34	0.61	7.9		4.41					286.0	248	252	1.15	0.049	1T,1A,1H
		3.05	0.44	6.8		4.12										
(3)	a rs	4.37	0.45	5.8	11.18	4.40					357.2	273	278	1.31	4.6-4	1T,1A,1H
		5.46	0.50		9.42	2.56	3.36		24.7	4.74						
(4)	a(z(rs)+rs)	5.28	0.46	0.9*	6.71	0.04	3.15	0.46=	8.1	4.59	311.1	271	278	1.15	0.047	2T,1A,1.5H
		4.86	0.42		6.53	0.00	1.82		7.1	2.16						
(5)	a(rs+rs)	4.50	0.44	8.3	10.59	3.80	1.18	0.44=		0.84	290.2	271	278	1.07	0.20	2T,1A,1H
		4.83	0.43		9.56	2.63		2.11	34.2	173						
(6)	a(z(cf)+rs)	4.74	0.37	0.9*	9.20	2.33	4.74=	1.15	30.0	150	285.3	271	278	1.05	0.26	1T,2A,1.5H
		4.65	0.30		8.82	2.01		0.65	26.6	129						
(7)	a(z(cf)+rs)	4.75	0.46	0.9*	8.78	2.02	4.75=	0.46=	26.7	172	292.3	272	278	1.08	0.19	1T,1A,1.5H
(8)	a(cf+rs)	4.50	0.33	8.1	10.75	3.68	4.50=	7.79		51	295.2	271	278	1.09	0.15	1T,2A,1H

See notes for Table 2.

integration (see Table 1). We first fitted isothermal models and found an excellent fit ($\chi^2_\nu = 0.80$ for $\nu = 148$; see T2.2) with a somewhat lower temperature, $kT = 3.68$ (3.08–4.34) keV, than the LAC data indicated, although the LAC temperature is within the 90% confidence upper limit. The derived fractional abundance $A = 1.50$ (0.94–2.28) is supersolar, substantially higher than that of the LAC spectrum. Fixing the abundance of the SSS spectra to match the half-solar value found in the LAC spectrum produced a significantly worse fit, with $\Delta\chi^2 = +15$ while $\Delta\nu = +1$; an F-test shows that the previous variable abundance fit is preferred with greater than 99.9% confidence. This is a strong indication of enhanced abundances in the SSS spectra relative to the more global LAC spectrum. WFJMA also noted a roughly cosmic abundance for the cooling flow component in the SSS data of this cluster, although no errors were given. They fitted a two-component emission model to the data, with one component being an isothermal model at the *EXOSAT*-derived temperature of 4.8 keV (Edge et al. 1990) and the other an isobaric cooling flow model. We also found the large column density of X-ray absorbing material previously found in the SSS spectra by WFJMA. The best-fit value for this model is $N_H = 1.2(1.0–1.5) \times 10^{21}$ cm^{-2}, which is twice the Galactic value interpolated from Stark et al. (1992), but we will show that the inferred amount is rather model dependent.

We also considered whether the high abundance seen in the SSS spectra may be an artifact of systematic errors in the ice model adopted for the SSS spectra. The generation of SSS response matrices depends on only one variable, the ice parameter appropriate for a given observation (see Table 1). The ice parameter has a maximum uncertainty of ± 0.4 during the time these data were taken (Christian et al. 1992). We reanalyzed the SSS spectra using a response matrix characterized by an ice parameter 0.4 larger than the best-estimate value used above. This increases the amount of ice assumed to be on the SSS entrance window, so the inferred internal absorption will be reduced: in refitting our isothermal model, the best-fit absorption was brought down to $N_H = 6.9(4.7–9.4) \times 10^{20}$ cm^{-2}, which is within $\sim 50\%$ of the Galactic value. The best-fit value of the fractional abundance was reduced to $A = 0.99$ (0.67–1.39), the 90% confidence range of which is still outside that of the more global LAC spectrum. Although systematic errors may make the absolute value of the central abundance somewhat insecure, the *existence* of a central enhancement seems more robust.

3.1.2. *Joint Spectral Fits*

Raymond-Smith models.—We next analyzed the LAC and SSS spectra jointly. The simplest plausible model is isothermal and assumes the SSS and LAC spectra are characterized by the same abundances and column density of cool absorbing matter. The normalizations were allowed to vary independently for the two instruments, to allow for their different fields of view. This model fitted poorly, with $\chi^2 = 203.3$ for $\nu = 169$ ($\chi^2_\nu = 1.20$; see T2.3). Allowing an additional spectral component with the same temperature and abundance but with an intrinsic absorbing column (at the redshift of the cluster) in addition to a fixed Galactic column provided only a marginally improved fit. (Note that for this and subsequent analysis of the other clusters, when we are not directly comparing to the work of Hatsukade 1989, we use Galactic values of N_H derived from Stark et al. 1992, using K. Arnaud's GETNH program.) A much better fit was provided by a two-temperature model in which the cooler component was allowed an intrinsic absorbing column in addition to a fixed Galactic column: $\chi^2 = 163.3$ for $\nu = 167$ (so $\chi^2_\nu = 0.98$ and $\Delta\chi^2 = -40$ for $\Delta\nu = -2$; see T2.4). In this model the cool component is attributed to the cooling flow and its normalization was constrained to be the same in the SSS and LAC fields of view, which assumes that the cooling flow emission is fully contained in each.

Finally, we allowed the abundance to vary independently in each of the two temperature components, which provided a significantly better fit, with $\chi^2 = 153.6$ for $\nu = 166$ ($\chi^2_\nu = 0.93$; see T2.5). The improvement over the single-abundance model of T2.4 ($\Delta\chi^2 = -9.7$ for $\Delta\nu = -1$) is significant with more than 99.8% confidence by the F-test. The best-fitting such two-temperature model is shown with the data in Figure 1, along with the residuals of the fit. This model has a hot component with $kT = 4.30$ (4.19–4.41) keV and a cooler component with $kT = 1.64$ (1.39–2.01) keV. The temperature χ^2 distributions are shown in Figure 2*a* where the dashed horizontal lines represent the single-parameter 90% and 99% confidence levels (corresponding to $\Delta\chi^2 = +2.71$ and $+6.63$, respectively). The temperature of the hotter component is $\sim 8\%$ greater than that derived from the LAC spectrum alone. The fractional abundance associated with the hotter component is $A_{\rm hot} = 0.47$ (0.42–0.53), while that of the cool component exceeds the cosmic value: $A_{\rm cool} = 2.63$ (1.01–>5). The χ^2 distributions for the abundances of the two temperature components are shown in Figure 3*a*, which shows that the abundance of the cool component, while having large errors, is nonetheless substantially greater than that of the hot component, at a confidence level of more than 99%. The ratio of model fluxes in the SSS and LAC fields of view is consistent with the ratio derived from IPC imaging data; the model fluxes were calculated in the 0.16–3.5 keV energy band appropriate to the background-subtracted, vignetting-corrected IPC images on the SAO CD-ROMs. The cooler spectral component of this model has an excess absorbing column density of $4.0(2.5–5.6) \times 10^{21}$ cm^{-2}, 9 times higher than the Galactic column. The N_H χ^2 distribution is illustrated in Figure 4*a*, where the Galactic value in the line of sight to A496 is also indicated. If the "intrinsic" absorption is distributed uniformly over the size of the cooling flow (with radius $R_{\rm cool} \approx 100$ kpc), there would be $\sim 9 \times 10^{11} M_\odot$ of cool material. We considered a model which allowed the covering fraction of absorbing material to vary and the subsequent best-fit value was unity (so the fit was not improved), with a 90% confidence lower limit of more than 83% coverage. However, since the intrinsic absorption is associated with the cool component in this spectral model, its total angular covering fraction may be substantially less than this if the cool emission component itself is clumped and the absorption is spatially correlated with the cool emission.

The column density associated with the cooler component of the two-temperature fit is 3 times larger than that inferred from the previous analysis of SSS spectra alone. This is because the best-fit temperature in the previous isothermal SSS analysis is larger than the temperature of the cooler component in the two-temperature fit and N_H is anticorrelated with the temperature: for a fixed spectral shape at low energies, the effect of reducing the temperature can be offset by increasing the absorbing column. This anticorrelation is illustrated in Figure 5, which shows the 1 σ, 90%, and 99% confidence contours for N_H versus kT in the previous isothermal fit to SSS data alone.

To test whether the intrinsic absorption is largely confined to the cooling flow (that is, within the SSS field of view), we considered a two-temperature, two-abundance model which

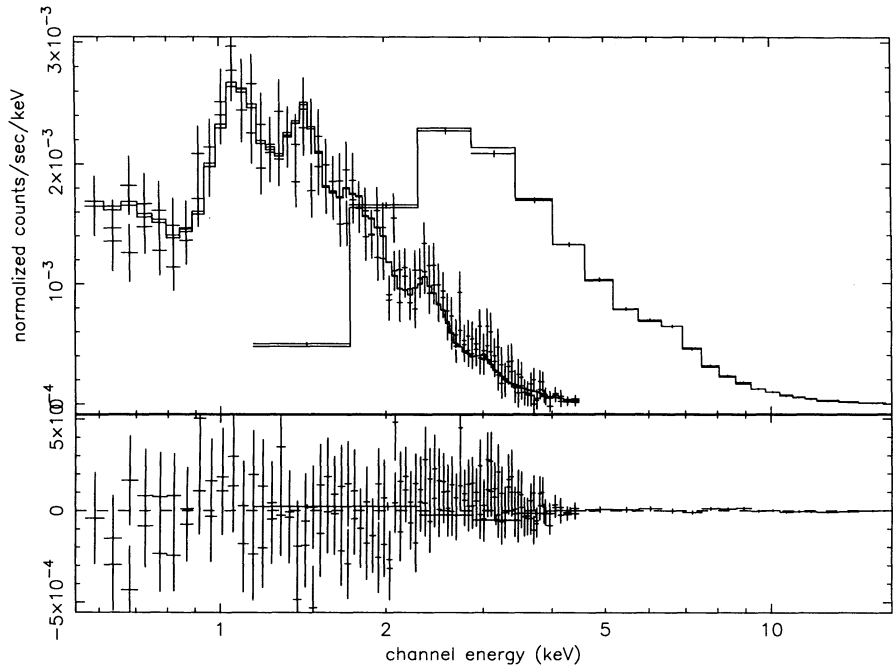

FIG. 1.—Two-temperature RS spectral models jointly fit to *Einstein* SSS and *Ginga* LAC data for A496; see line 5 of Table 2 for best-fit parameters

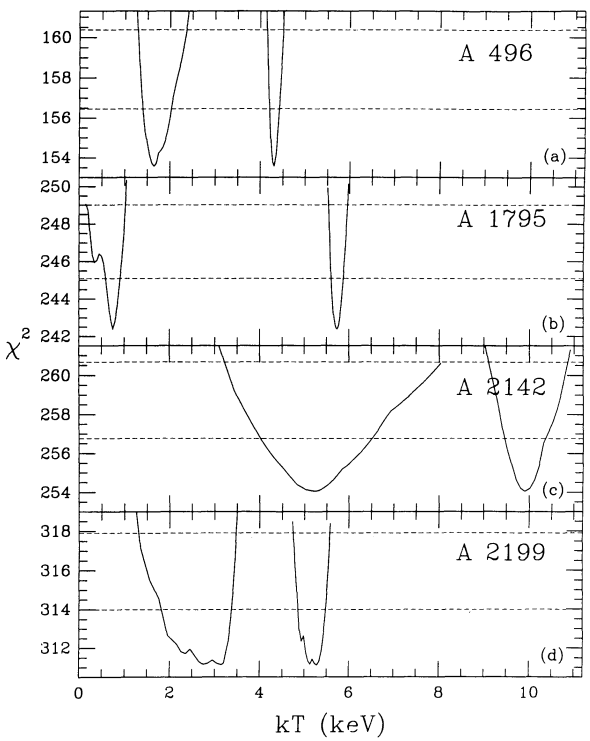

FIG. 2.—Temperature (kT, in keV) χ^2 distributions for two-temperature RS models: (*a*) A496; (*b*) A1795; (*c*) A2142; (*d*) A2199. The lower and upper dashed lines are the 90% and 99% confidence levels, corresponding to $\Delta\chi^2 = 2.71$ and 6.63, respectively.

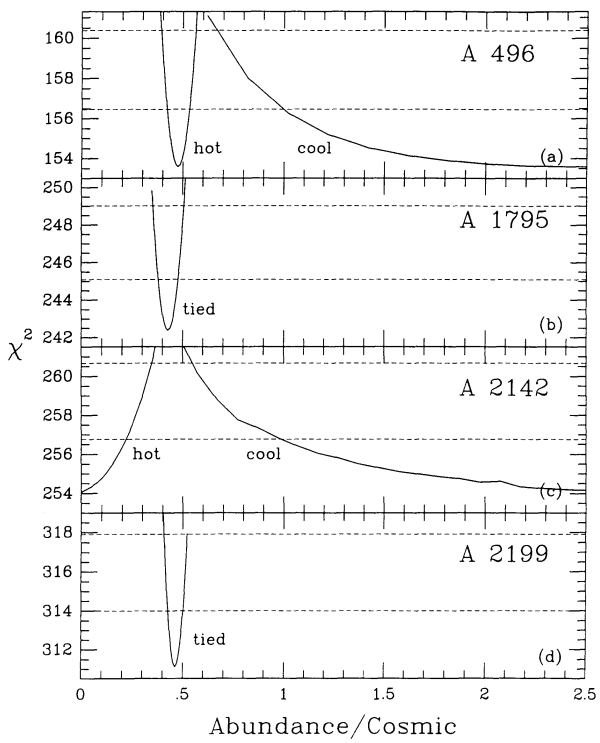

FIG. 3.—χ^2 distributions for the abundance(s) of the hot and cool components in the two-temperature RS models for: (*a*) A496; (*b*) A1795 (abundances of the two temperature components were set equal); (*c*) A2142; (*d*) A2199 (abundances of the two temperature components were set equal).

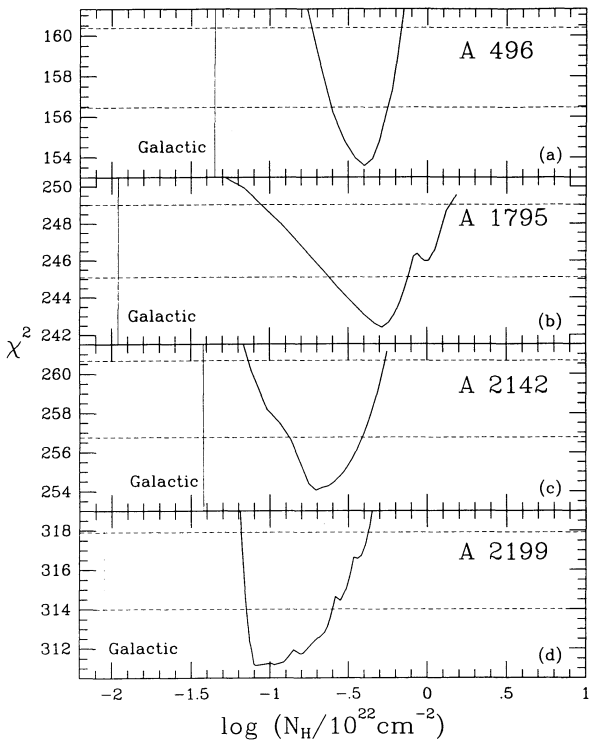

FIG. 4.—χ^2 distributions for the "intrinsic" hydrogen column density associated with the cooler spectral component of the two-temperature RS models for: (*a*) A496; (*b*) A1795; (*c*) A2142; (*d*) A2199. Galactic values are also indicated by vertical lines.

allowed only one global value of absorbing column to be fit. The best-fitting such model is only marginally worse than the best model illustrated above, having $\Delta\chi^2 = +3.9$ for $\Delta v = 0$ (see T2.6), but the best-fit value of N_H is more than twice the Galactic value. This value is very close to that found in the previously described fit to the SSS data alone, which illustrates the insensitivity of the LAC data to N_H. Thus, we cannot demonstrate that the extra absorption is confined to the SSS field of view. However, it is unreasonable for the extra absorption to be due to an error in the estimate of the Galactic component, since typical errors in interpolating Galactic values on small angular scales from broad-beam surveys such as that of Stark et al. (1992) are only of order 10^{20} cm^{-2} (Elvis et al. 1986).

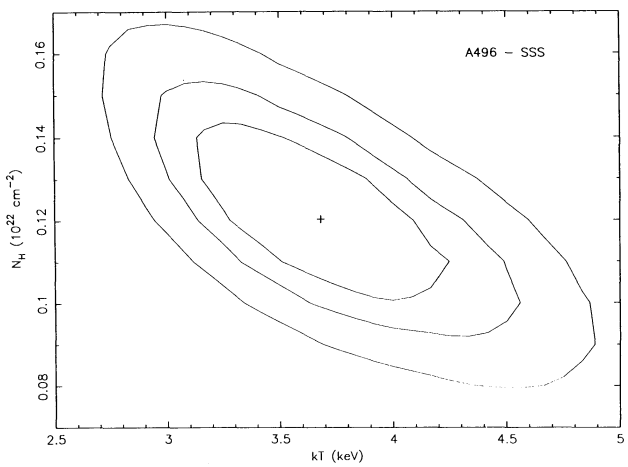

FIG. 5.—N_H-kT contours for isothermal fit to SSS data of A496

Although the model illustrated in Figures 1 and 2*a*–4*a* provides an excellent fit to the LAC and SSS data, inspection of the χ^2 residuals for the best-fitting two-temperature model above shows structure in the lowest-energy LAC channels which may suggest that the LAC sees somewhat more cool emission than the SSS. To test whether the bulk of the cool component is confined within the SSS field of view, we allowed the LAC and SSS normalizations for the cool components to vary independently. The resulting respective normalizations were the same within their errors and the fit was not significantly improved. In an additional test, we added a third temperature component to the model which could contribute only to the LAC spectrum. This LAC-only component ended up being very cool ($kT \approx 1$ keV) and significantly improved the fit, reducing χ^2 by ~ 12. However, this cool component contributed only 1%–2% of the flux in the LAC passband, which is at the level expected from calibration uncertainties and unresolved background sources; thus there is little evidence of cool emission outside the SSS field of view. *ROSAT* imaging data will be incorporated in a subsequent paper.

Cooling flow models.—In the previous two-temperature analysis we attributed the cooler of two temperature components to the cooling flow at the center of A496. However, a cooling flow spectrum is only roughly approximated by a single-temperature RS thermal model. We therefore investigated models incorporating a more realistic cooling flow spectral component in order to constrain the accretion rate and to assess the model dependence of the high metal abundances and absorption columns we deduce for the cool component. We adopted the cooling flow spectral model of Mushotzky & Szymkowiak (1988), in its most recent implementation in XSPEC (vers. 8.33). There are six variables in the cooling flow model: the temperature from which gas cools T_{high}, the temperature to which gas cools T_{low}, the accretion rate M (which is the normalization), the fractional metal abundance A, the redshift z, and a slope parameter s for a temperature-dependent weighting of the isobaric emission measure versus temperature relation (the slope is zero for an isobaric cooling flow). The bulk of the cooling flow emission will be radiated under roughly isobaric conditions in the outer half of the cooling flow. We find from XSPEC simulations that pure cooling flow spectra (with T_{low} below X-ray–emitting temperatures) are fitted reasonably well by isothermal RS models with temperatures $\sim$2–3 times smaller than T_{high} (also see White & Sarazin 1987). The cooler component in the previously discussed two-temperature model thus has roughly the temperature one expects from a cooling flow starting at the higher of the two temperatures.

In our fits incorporating a cooling flow spectrum, we couple the cooling flow model to a RS isothermal model for the cluster emission exterior to the cooling flow. As with the previous two-temperature fits, we included a (fixed) Galactic absorption component, and we associated an additional (variable) "intrinsic" absorption component with the cooling flow. In the cooling flow model we set T_{high} equal to the temperature of the exterior isothermal component, we fixed T_{low} at 0.1 keV (below the bulk of X-ray emitting energies), fixed the redshift, and set the cooling flow slope parameter to zero (for isobaric flow). The accretion rate, the abundances of the cooling flow and the exterior RS components, and the intrinsic absorption freely

varied, while T_{high} was tied to and varied with the temperature of the exterior RS component.

We found an excellent fit for a model in which the cooling flow normalizations were the same for the SSS and LAC: $\chi^2_\nu = 0.91$ for $\nu = 167$ (see T2.7), which has $\Delta\chi^2 = -1.9$ (for $\Delta\nu = +1$) compared to the best two-temperature RS model with tied cool component normalizations. The accretion rate was found to be 154 (127–188) $M_\odot$ yr^{-1}, consistent with previous determinations, but with smaller errors. The abundance of the cooling flow, $A_{cf} = 3.79$ (1.58– > 9), was found to be significantly greater than that of the exterior gas, $A_{hot} = 0.25$ (0.16–0.37). The χ^2 distributions for the abundances of the two spectral components are shown in Figure 6*a*. Despite its large error, the cooling flow abundance is greater than that of exterior gas at more than 99% confidence, which is consistent with the results of the previous two-temperature analysis. The ratio of model fluxes in the SSS and LAC fields of view are again consistent with that derived from IPC imaging data. The best-fitting value of intrinsic N_H is very close to that of the previous analysis: $N_H = 3.8(3.2–4.6) \times 10^{21}$ cm^{-2}. Using a similar RS plus cooling flow spectral model (but with the cluster temperature fixed), WFJMA found a lower value for the intrinsic column density: $N_H = 2 \times 10^{21}$ cm^{-2}. This disparity is largely due to WFJMA adopting the *EXOSAT*-derived temperature of 4.8 keV (Edge et al. 1990), which is ~15%–20% higher than that derived by the higher quality *Ginga* spectrum. We further assessed the significance of the relatively enhanced cooling flow abundance by considering a model with only a single variable abundance for both the cooling flow and RS components. This model (see T2.8) produced a significantly larger χ^2 ($\Delta\chi^2 = +17$ for $\Delta\nu = +1$) than the dual-abundance model of T2.7, which is preferred with 99.99% confidence with the *F*-test. To test whether the extra absorption component is confined to the SSS field of view, we considered a model with one variable global value of N_H (see T2.9), rather than a variable absorption component intrinsic to the cooling flow; this provided a much worse fit ($\Delta\chi^2 = +40$ for $\Delta\nu = 0$) than the model of T2.7. This suggests that the extra absorption is mostly confined to the SSS field of view (but recall that a similar global–N_H model employed in a previous dual-RS fit [T2.6] did *not* show such a pronounced degradation in the quality of the fit). A model allowing a partial covering fraction for the intrinsic absorption produced a best-fit value of unity and a 90% confidence lower limit of more than 85% coverage. To assess whether the cooling flow emission extends outside the SSS field of view, we allowed the LAC and SSS cooling flow normalizations to vary independently. The fit was not significantly improved.

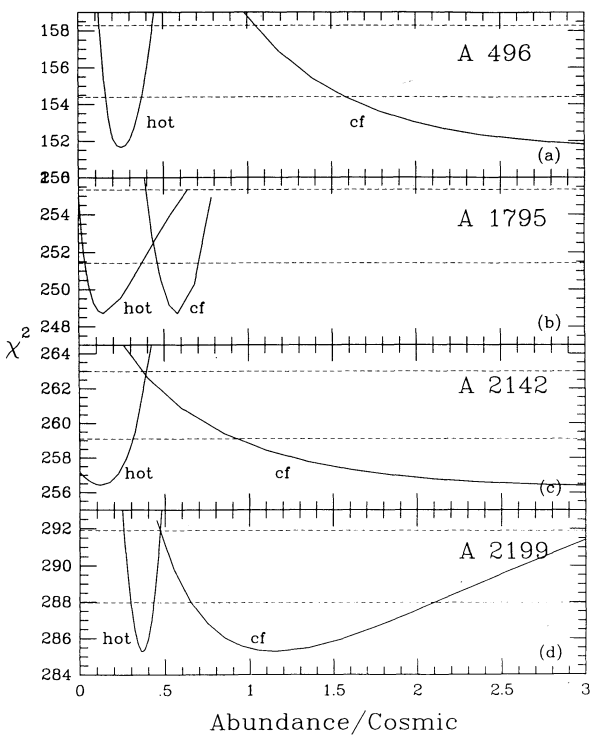

FIG. 6.—χ^2 distributions for abundances of cooling flow (cf) and RS (hot) components of joint fits to LAC and SSS spectra. (*a*) A496; (*b*) A1795; (*c*) A2142; (*d*) A2199.

We conclude that A496 has a cool component attributable to a central cooling flow. This cool component is associated with a large column density of X-ray absorbing material, but these data do not unambiguously show that it is confined to the SSS field of view. There appears to be an abundance gradient in A496, with abundances substantially larger at the center and declining outward. The amount of metals in the cooling flow is far larger than what could be produced by present levels of stellar mass loss; however, the metals could have been produced during the integrated history of mass loss in the central dominant galaxy and other galaxies in the core. There does not appear to be much cool emission outside the SSS field of view.

3.2. *Abell 1795*

Abell 1795 is a Bautz-Morgan Type I cluster with a central cD. At a redshift $z = 0.0620$, the cluster has a luminosity distance of 377 h_{50}^{-1} Mpc, and $1' = 96$ h_{50}^{-1} kpc (for an angular diameter distance of 335 h_{50}^{-1} Mpc). The central cD has a significant peculiar velocity, 370 km s^{-1}, given its cluster velocity dispersion of $\sigma = 773$ km s^{-1} (ZHG; Gebhardt & Beers 1991); more general velocity substructure is not apparent in its velocity histogram (ZHG). In the inner parts of the central cD, McNamara & O'Connell (1992) found a pronounced optical color gradient relative to that expected from a normal giant elliptical and attributed this to ongoing star formation in the surrounding cooling flow.

Einstein IPC X-ray imaging analyses find accretion rates ranging from ~340–400 $M_\odot$ yr^{-1} (Stewart et al. 1984; Arnaud & Fabian 1987). This range is similar to that deduced from SSS spectra by Mushotzky (1984) and Mushotzky & Szymkowiak (1988): 425–560 $M_\odot$ yr^{-1}. Arnaud & Fabian (1987) find a cooling radius of ~2′.2, well within the SSS field of view. The long optical filament discovered by CHJY (extending to ~45″ from near the center), which may be a cooling flow condensate, is also well within the SSS field of view.

IPC images of A1795 show that there are several compact sources in the LAC field of view (but outside the SSS field of view). The brightest of these sources is a Seyfert 1 galaxy (EXO 1346.2+2645). The flux from these sources is $\lesssim$3% of the total is the *Einstein* passband, so their presence does not effect these spectral fits significantly. The nominal center of the SSS pointing is within 0′.6 of the IPC X-ray peak, while the nominal center of the LAC pointing is within 8′ of the X-ray peak.

3.2.1. *Separate LAC and SSS Spectral Fits*

The previous LAC analysis of Hatsukade (1989) found a collisional ionization equilibrium model temperature of

$kT = 5.34$ (5.23–5.45) keV and an (adjusted) fractional iron abundance $A = 0.46$ (0.41–0.51), for an assumed Galactic hydrogen column of $N_H = 1.7 \times 10^{20}$ cm^{-2}. We fitted a RS isothermal model to the LAC spectrum alone with the same value of N_H and found a slightly higher temperature and lower abundance: $kT = 5.57$ (5.45–5.69) keV and $A = 0.43$ (0.38–0.48), with 90% confidence intervals which overlap those of Hatsukade (see T3.1). If the hydrogen column density is allowed to vary freely, it is not well determined; the smallest χ^2 is associated with zero column, but χ^2 is reduced by only 2.4 for $\Delta\nu = -1$.

Of the six SSS spectra available for A1795, we analyzed three. Two of the omitted SSS spectra had ice variations of $\sim 50\%$ in the course of their integrations and the third omitted spectrum had twice as much ice as the remaining three (see Table 1). Our isothermal model fits to the SSS spectra have significantly lower temperatures than found in the LAC spectrum. With the abundance free to vary, the best-fitting temperature of an adequate fit ($\chi^2_\nu = 1.07$ for $\nu = 225$) is 3.67 (3.26–4.14) keV. The abundance is very low and poorly constrained, with a 90% confidence upper bound of 0.24 cosmic and no lower bound (see T3.2). However, fixing the abundance to that indicated in the LAC spectrum significantly worsened the fit ($\Delta\chi^2 = +9$ for $\Delta\nu = +1$; $\chi^2_\nu = 1.11$); an F-test shows that the previous fit with variable abundance is significantly better at the 99.5% confidence level.

3.2.2. *Joint Spectral Fits*

Raymond-Smith models.—Having the SSS spectra characterized by a temperature lower than that of the LAC spectrum motivated a two-temperature model jointly fit to the SSS and LAC data. This provided an improvement in χ^2_ν. The model is nearly the same type as used in A496, incorporating a fixed Galactic absorption column and an additional variable absorption component associated with the cooler of the two temperature components. As before, the additional "intrinsic" absorption was assumed to be at the redshift of the cluster. In this cluster, however, the abundance of the cool component was tied to that of the hot component since the SSS data provided such a poor constraint on the abundance. In modeling a cool component associated with the central cooling flow, we can safely assume that the SSS field of view encompasses all of the cooling flow emission, given the distance to A1795. (There is still the possibility of cool emission in the outer parts of the cluster where it could be detected by the LAC, but only a small projected portion of which would be detected by the SSS). The best-fitting model is quite good ($\chi^2_\nu = 0.99$, $\nu = 244$) and is illustrated with the data in Figure 7. The temperatures of the two components are $kT = 5.73$ (5.59–5.87) keV and $kT = 0.74$ (0.58–0.90) keV (see T3.4); their χ^2 distributions are shown in Figure 2*b*. The overall fractional abundance is $A = 0.43$ (0.338–0.48) and its χ^2 distribution is illustrated in Figure 3*b*. When we allowed the abundance of the cool component to vary independently of that of the hot component, we found that the fit was not improved and the cool abundance was poorly constrained. Thus, these RS models provided no evidence of centrally enhanced abundances. The ratio of model fluxes in the SSS and LAC fields of view is consistent with that derived from IPC imaging data. A substantial absorbing column is associated with the cool component, $N_H = 5.1$ (2.4–7.6) $\times 10^{21}$ cm^{-2}, which is ~ 45 times larger than the line-of-sight Galactic column; Figure 4*b* shows the N_H χ^2 distribution. As we show below, this high value of N_H is very model dependent, with much lower values provided by models incorporating cooling flow spectra.

This model provided a significantly better fit than simpler alternatives, the simplest being characterized by a single temperature, abundance, and absorbing column. The best-fitting such model (see T3.3) had $\Delta\chi^2 = +42$ (for $\Delta\nu = +2$) relative to the previous two-temperature model. We further tested the significance of the cooler component by forcing the temperatures of the two components to be the same, but allowing one of the isothermal components to have intrinsic absorption at the cluster redshift (in addition to an overall absorption

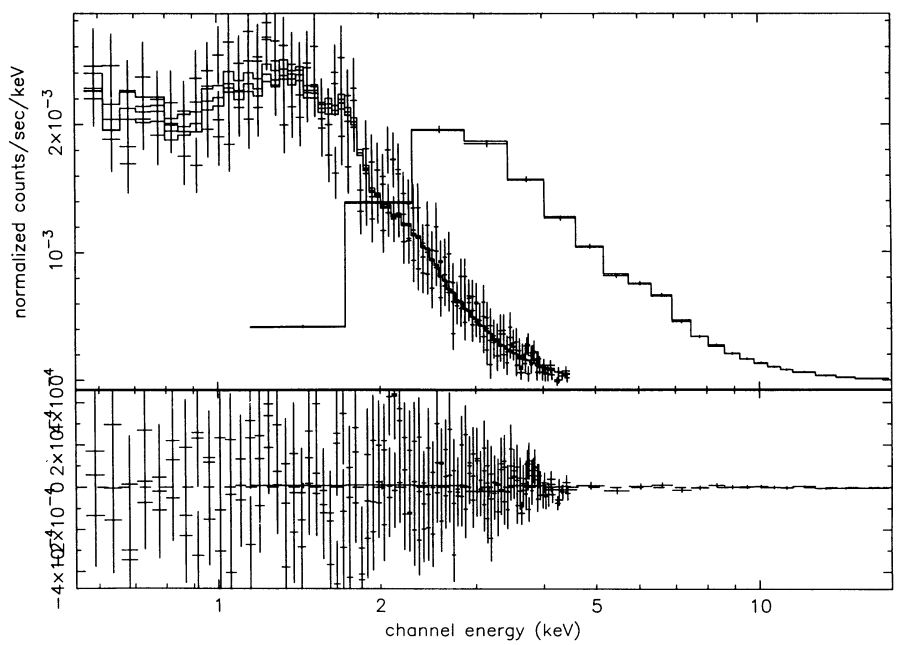

FIG. 7.—Two-temperature RS spectral models jointly fit to *Einstein* SSS and *Ginga* LAC data for A1795; see line 4 of Table 3 for best-fit parameters

fixed at the Galactic value). The best-fitting such model had $\Delta\chi^2 = +46$ (for $\Delta\nu = +1$) compared to the previous two-temperature model with intrinsic absorption. The need for a cooler component is evidently extremely significant: the F-test shows that the improvement provided by the second temperature component is significant with more than 99.99% confidence. We tested whether the "intrinsic" absorbing column is confined to the SSS field of view by forcing the two-temperature model to have only one global value of N_H. The best-fitting such model had $N_H = 3 \times 10^{20}$ cm^{-2}, 3 times the Galactic value, but provided a somewhat poorer fit, with $\Delta\chi^2 = +6.2$ for $\Delta\nu = 0$. The poorer fit is weak evidence for the extra absorption being confined to the SSS field of view, but the value of N_H is consistent with that indicated in the isothermal analysis of the SSS data alone (see T3.2), so the LAC data again provide a poor constraint on N_H and its coverage. We also considered a partial coverage model for the intrinsic absorption component (in a spectral model otherwise like that of T3.4) and found the best-fit value of the covering fraction to be unity (so the fit was not improved), with a 90% confidence lower limit of more than 80% coverage.

As for A496, we tested whether the LAC saw significantly more cool emission than was in the SSS field of view by adding a third RS component to the LAC spectral model. The resulting best-fit χ^2 was not significantly improved and the contribution of the (cool) third component to the LAC passband was only $\sim 1\%$. As we saw before in A496, this is at the level expected from calibration uncertainties and unresolved background sources.

Cooling flow models.—Since a central cool component was strongly indicated above, we also considered a spectral model incorporating a cooling flow component in order to constrain its accretion rate and assess the model dependence of the intrinsic N_H. Given the lack of evidence of enhanced abundances in the SSS spectra relative to the LAC spectrum, we initially tied the abundances of the two spectral components together. The cooling flow normalization $\dot{M}$ was taken to be the same in the LAC and SSS spectra. The best-fitting model is quite good, although not quite as good as the best-fitting two-temperature model described above: in this case, $\chi^2/\nu = 252.6/245$ ($\chi^2_\nu = 1.03$; see T3.5), so compared to the better fitting two-temperature model (T3.4), $\Delta\chi^2 = +10$ for $\Delta\nu = +1$. The exterior temperature, $kT = 6.07$ (5.85–6.33) keV, is $\sim 9\%$ larger than in the previous two-temperature RS model. The fractional abundance $A = 0.45$ (0.40–0.50) is the same as derived previously. The intrinsic absorption, $N_H = 8.9(5.8\text{–}11.5) \times 10^{20}$ cm^{-2} is ~ 6 times smaller than that associated with the cool component of the previous model; this is still ~ 8 times larger than the Galactic column in this line of sight and $\sim 10\%$ larger than the value found by WFJMA. The accretion rate is consistent with previous estimates: $\dot{M} = 411$ (290–533) $M_\odot$ yr^{-1}.

When we allowed the abundances of the cooling flow and RS components to vary independently, a slightly better fit was achieved, with $\Delta\chi^2 = -3.9$ for $\Delta\nu = -1$ (see T3.6); this improvement is significant at the 95% level by the F-test. The cooling flow abundance $A_{cf} = 0.58$ (0.46–0.71) ended up significantly larger than that of the hot component $A_{hot} = 0.14$ (0.04–0.37), with nonoverlapping 90% limits, but A_{hot} is poorly determined. The χ^2 distributions for the abundances of the two spectral components are shown in Figure 6*b*. The ratio of model fluxes in the SSS and LAC fields of view is consistent with that derived from IPC imaging. We also tested whether this model allows the extra absorbing column to be confined to the SSS field of view: allowing only a global value of N_H led to a slightly worse fit, with $\Delta\chi^2 = +1.6$ for $\Delta\nu = 0$. The best-fit global value of N_H is ~ 4 times higher than the Galactic value (see T3.7) and several times higher than the plausible uncertainty in the Galactic value. However, given the comparable quality of the fit, we cannot prove that the extra absorption is confined to the SSS field of view. We also considered a partial covering model for the intrinsic absorption (in a model otherwise like that of T3.6) and found the best-fit value to be unity (so the fit was not improved), and the 90% confidence lower limit was greater than 45% coverage.

We conclude that there is a cool spectral component attributable to a cooling flow in A1795. In contrast to A496, the evidence is mixed on there being a significant central abundance enhancement: the dual-temperature RS models show no evidence of a significant enhancement, while the poorer fitting cooling flow models do show evidence of an enhancement. We found the amount of cool, X-ray absorbing material first found by WFJMA to be rather model dependent, but still very substantial. We found no evidence in this data of the LAC seeing significantly more cool emission than the SSS.

3.3. *Abell 2142*

Abell 2142 is a Bautz-Morgan type II cluster, with a dominant pair of giant ellipticals at its center (Rood-Sastry type B), one of which has multiple nuclei (Hoessel 1980). With a redshift $z = 0.0899$, the cluster is the most distant in our sample: it has a luminosity distance of 551 h_{50}^{-1} Mpc, so $1' = 132\ h_{50}^{-1}$ kpc (for an angular diameter distance of 464 h_{50}^{-1} Mpc).

X-ray imaging analysis indicated the absence of a cooling flow with an accretion rate of $\sim 55\ M_\odot$ yr^{-1} (Arnaud & Fabian 1987) and a cooling radius of $\sim 0'.7$. Previous analysis of SSS spectra provided an upper limit to the cooling flow accretion rate of $\dot{M} < 540\ M_\odot$ yr^{-1} (Mushotzky & Szymkowiak 1988). Since the cooling flow is contained in only $\sim 5\%$ of the SSS field of view, its emission is heavily diluted by hotter exterior gas.

The IPC image has three other sources in the *Ginga* field of view which are outside the SSS field of view: a K5 star (SAO 84114) and a Seyfert 1 galaxy (1556+259) very close together on the sky (Reichert et al. 1982) and a QSO (1557+272). They contribute only $\sim 2\%$ of the flux in the IPC field, so their contribution is negligible compared to that of the cooling flow. The nominal center of the SSS pointing is $0'.53$ from the IPC X-ray peak, while that of the LAC is $3'.6$ away.

3.3.1. *Separate LAC and SSS Spectral Fits*

Hatsukade (1989) previously found a temperature of $kT = 8.68$ (8.48–8.88) keV and an abundance of 0.35 (0.30–0.40) cosmic in the LAC spectrum. Our best-fitting RS isothermal model using the same value of N_H has a slightly larger temperature $kT = 8.99$ (8.78–9.18) and virtually identical fractional abundance $A = 0.34$ (0.29–0.39) (see T4.1). This isothermal model provides a formally excellent fit, with $\chi^2_\nu = 0.85$ for $\nu = 21$ (see T4.1). When N_H is allowed to vary freely, it is poorly determined and χ^2 is not significantly improved.

We also analyzed the three SSS spectra available for this cluster. We first fitted isothermal models and found an excellent fit ($\chi^2_\nu = 0.94$, $\nu = 248$; see T4.2) with a temperature of $kT = 7.81$ (6.74–9.01) keV; the 90% confidence upper limit encompasses the LAC-derived temperature. However, the derived fractional abundance $A = 1.97$ (1.08–3.26) is much

higher than that indicated in the LAC spectrum and the hydrogen column of 8.4(7.2–9.5) $\times 10^{20}$ cm^{-2} is about twice the Galactic value. A χ^2 contour of kT–A shows that the abundance enhancement is not the result of temperature uncertainties, since there is a firm 99% confidence lower limit of $A \gtrsim 0.5$. Fixing the model abundance to match the smaller value found in the LAC spectrum produced a significantly worse fit ($\Delta\chi^2 = +11.6$, for $\Delta\nu = +1$), which is rejected relative to the former model (in T4.2) at the 99.5% confidence level by the F-test.

As for A496, we assessed whether the supersolar abundance may be due to systematic errors in the SSS ice model. The maximum uncertainty in the ice parameter for these data is again ± 0.4, so we again employed response matrices which were characterized by ice parameters 0.4 larger than the best-estimate value used above. The subsequent best-fitting isothermal RS model had a smaller abundance, $A = 0.71$ (0.44–1.04); however, its 90% confidence range is still outside that of the more global LAC spectrum. This is a strong indication that abundances are enhanced in the SSS field of view relative to exterior gas. The absorbing column was reduced to $N_{\rm H} = 2.8$ (1.5–4.1) $\times 10^{20}$ cm^{-2}, which is consistent with the Galactic value.

3.3.2. *Joint Spectral Fits*

Raymond-Smith models.—In a joint analysis of the SSS and LAC spectra, we found a formally good fit for the simplest plausible RS model, characterized by a single temperature, abundance, and column density ($\chi^2_\nu = 0.98$, $\nu = 271$; see T4.3), although the best-fit "global" $N_{\rm H}$ is twice the Galactic column. Since the SSS data alone seem to require roughly cosmic abundances, while the LAC data require abundances which are one third as much, we also considered a dual RS model with the same temperature but with independently varying abundances. We found a somewhat improved fit ($\Delta\chi^2 = -6.6$ for $\Delta\nu = -2$; see T4.4), but the abundance of the dominant RS component (with normalization dictated by the LAC) vanished. This means that virtually all of the line emission seen by the LAC could conceivably come from within a region defined by the SSS field of view, leaving few metals to the exterior. The fractional abundance of the component within the SSS field of view is $A_{\rm inner} = 2.35$ (0.99–>4), while the 90% upper limit to the outer component fractional abundance is $A_{\rm outer} \lesssim 0.20$.

A two-temperature model with separately variable abundances (see T4.5) provided an additional improvement on this already acceptable fit, giving $\chi^2_\nu = 0.95$ or $\Delta\chi^2 = -5.4$ for $\Delta\nu = -1$ relative to the previous model in T4.4; this improvement is significant at the 98% level by the F-test. Once again, however, the dominant component (now hotter) has a vanishing abundance (with a 90% confidence upper limit of $A_{\rm hot} \lesssim 0.22$ solar). This model and the data are shown in Figure 8. The χ^2 distributions for the temperatures of the two RS components are shown in Figure 2*c*. The temperature of the hot component is $\sim 10\%$ greater than that derived from the LAC data alone. The χ^2 distributions for the hot and cool abundances are shown in Figure 3*c*, where it is clear that the abundances differ with greater than 99% confidence. This model also required an intrinsic absorbing column of ~ 5 times the line-of-sight Galactic value: $N_{\rm H} = 2.0(1.3–3.9) \times 10^{21}$ cm^{-2}; the $N_{\rm H}\chi^2$ distribution is shown in Figure 4*c*. The ratio of model fluxes in the SSS and LAC fields of view is consistent with that derived from IPC imaging.

Fixing the abundance of the hot component to be equal to that derived from the LAC data alone provided an acceptable fit ($\chi^2_\nu = 0.97$ for $\nu = 269$; see T4.6) although with some degradation compared to the previous model with vanishing abundances: $\Delta\chi^2 = +6.3$ for $\Delta\nu = +1$. The fractional abundance of the cool component remained relatively high, with a 90% confidence interval which just touched that of LAC data analyzed alone: $A_{\rm cool} = 0.97$ (0.39–2.35). Finally, the need for two abundances was further tested by forcing the cool and hot components to have the same abundances. The best fit (see T4.7)

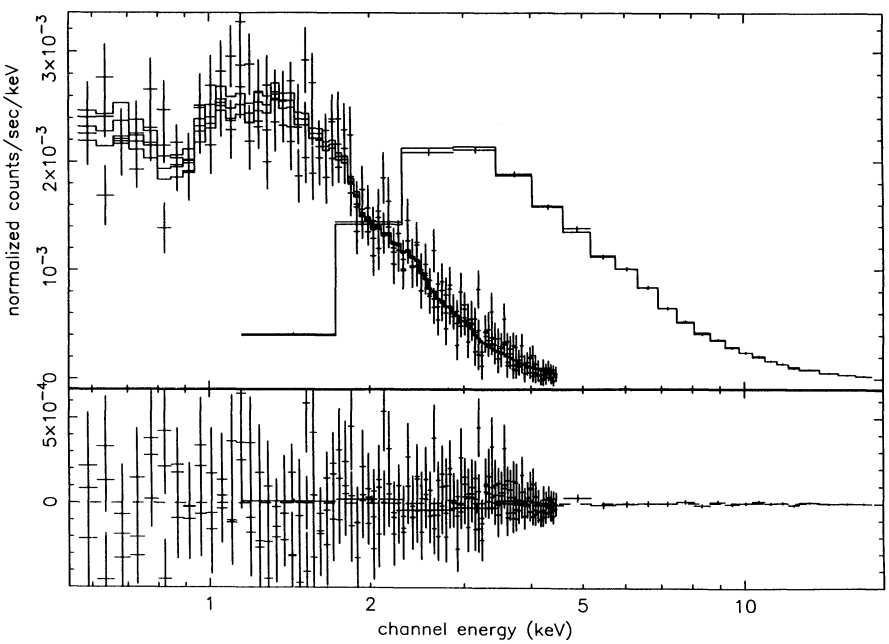

FIG. 8.—Two-temperature RS spectral models jointly fit to *Einstein* SSS and *Ginga* LAC data for A2142; see Line 4 of Table 4 for best-fit parameters

had $\Delta\chi^2 = +8.9$ for $\Delta\nu = +1$ relative to the dual-abundance model in T4.5; the need for the additional abundance component is significant at the 99.7% confidence level by the F-test.

We tested whether the substantial intrinsic absorbing column required above is confined to the SSS field of view by fitting a two-temperature, two-abundance model with only one (variable) global column density. The resulting best fit is nearly as good as that detailed in T4.5 ($\Delta\chi = +1.3$ for $\Delta\nu = 0$), so we cannot demonstrate that the absorption is confined to the SSS field of view. However, the best-fitting N_H is twice as high as the Galactic value, 8 times larger than its likely uncertainty. We also explored a partial covering fraction model for the intrinsic absorption: the best-fit value of the covering fraction was unity (so the fit was not improved), with a 90% confidence lower limit of $\sim 60\%$.

Cooling flow models.—We also investigated spectral models incorporating a cooling flow component in order to constrain its accretion rate. A RS model plus the standard cooling model employed for the previous clusters provided about as good a fit as the best-fitting dual RS models, with $\chi^2_\nu = 0.95$ for $\nu = 269$ (see T4.8). The abundance of the RS model exterior to the cooling flow was again very low, with $A_{\rm hot} = 0.12$ (0–0.32), while the cooling flow component has a supersolar abundance with large errors: $A_{\rm cf} = 3.6$ (0.93–>5.6); the χ^2 distributions for the abundances of these two spectral components are shown in Figure 6*c*. The accretion rate is $\dot{M} = 439$ (345–545) $M_\odot$ yr^{-1}, substantially higher than that derived from the imaging analysis of Arnaud & Fabian (1987). Substantial intrinsic absorption is again indicated, with a higher column than in the previous dual RS fits: $N_H = 3.5$ (3.4–5.5) $\times 10^{21}$ cm^{-2}. This is several times higher than the intrinsic column found by WFJMA. The SSS/LAC model flux ratio for this model is consistent with that derived from IPC imaging.

Forcing the abundances of the cooling flow and exterior RS components to be equal degraded the quality of the fit somewhat ($\Delta\chi^2 = +6.4$ for $\Delta\nu = +1$; see T4.9); the former dual-abundance model (T4.8) is preferable at the 99% confidence level by the F-test. As we did for the dual RS models, we also tested whether the intrinsic absorbing column is confined to the SSS field of view: still keeping the abundances of the two spectral components tied, we allowed only one globally varying absorbing column and found little additional degradation in the best fit (see T4.10), so we cannot prove that the absorption is confined to the SSS field of view. Nonetheless, the best-fitting global absorbing column was about twice the nominal Galactic value, just as we found in the dual RS test, so the excess absorption is several times larger than the likely error in the Galactic column. The best-fitting accretion rate, $\dot{M} = 177\ M_\odot$ yr^{-1}, is less than half that derived in models which allowed for an intrinsic absorption component. We also considered a partial covering fraction model for the intrinsic absorption; in a model similar to that of T4.8, we found a best-fit value of unity for the covering fraction (so the fit was not improved), with a 90% confidence lower limit of more than 80%.

We conclude from these various spectral model fits that there is strong spectral evidence for a relatively cool central component in A2142 and that its abundance is likely to be enhanced relative to that of exterior gas, although its absolute level is somewhat uncertain due to SSS ice parameter uncertainties. We found that the amount of intrinsic absorption previously found by WFJMA, although large, is rather model dependent. The spectrally derived cooling accretion rate depends sensitively upon how the intrinsic absorption is distributed.

3.4. *Abell 2199*

A2199 is a cD cluster of Bautz-Morgan Type I. The central cD, NGC 6166, has a triple nucleus (Hoessel 1980), one of which contains unresolved Hα emission (CHJY). At a redshift $z = 0.0309$, the luminosity distance is 187 h_{50}^{-1} Mpc, the closest in our sample, and $1' = 51\ h_{50}^{-1}$ kpc (for an angular diameter distance of 176 h_{50}^{-1} Mpc). There is pronounced asymmetry in the cluster's histogram of galaxy velocities (ZHG) and NGC 6166 has a peculiar velocity of ~ 380 km s^{-1} relative to the cluster mean. ZHG found this peculiar velocity to be significant compared to the cluster velocity dispersion of 794 km s^{-1}, but Gebhardt & Beers (1991), using a more robust statistical test, suggest otherwise. McNamara & O'Connell (1992) found photometric evidence of ongoing star formation in the central cD: a modest optical color gradient relative to the color profiles of "normal," non–star-forming template ellipticals.

X-ray imaging studies indicate the presence of a central cooling flow with an accretion rate of ~ 100–$220\ M_\odot$ yr^{-1} (Stewart et al. 1984; Arnaud & Fabian 1987; Thomas et al. 1987). Cooling radius estimates range from 3.2–6.7 (Arnaud & Fabian 1987; Thomas et al. 1987), extending beyond the 3′ radius of the SSS field of view. However, as noted for A496, if the system age were $\lesssim 10^{10}$ yr, rather than the 2×10^{10} yr adopted in these studies, the cooling radius may be within the SSS field of view. Mushotzky (1984) and Mushotzky & Szymkowiak (1988) deduce an accretion rate of ~ 45—$60\ M_\odot$ yr^{-1} from SSS spectra. No serendipitous sources significant enough to affect this study appear in the IPC image of this cluster. The nominal center of the SSS field is 0.10 from the IPC X-ray peak, while that of the LAC is 10.7 away.

3.4.1. *Separate LAC and SSS Spectral Fits*

A RS isothermal spectral model fit to the LAC data alone provides an adequate fit ($\chi^2_\nu = 1.10$ for $\nu = 22$) with a temperature $kT = 4.48$ (4.41–4.54) keV and a fractional abundance $A = 0.43$ (0.39–0.46) (see T5.1). Fixing the absorbing column to the very low Galactic value ($\sim 9 \times 10^{19}$ cm^{-2}), rather than allowing it to be fit freely, increased χ^2 by 1.4 (while $\Delta\nu = +1$), so there was little significant effect.

There are three SSS spectra and all have good ice parameters. The best-fitting isothermal model provided a mediocre fit, with $\chi^2_\nu = 1.15$ for $\nu = 248$ (see T5.2). The temperature $kT = 3.34$ (3.05–3.70) keV is 25% lower than that derived from the LAC spectrum and the respective 90% confidence χ^2 limits do not overlap. The fractional abundance, $A = 0.61$ (0.44–0.82) may be somewhat higher than that indicated in the LAC spectrum, but the 90% confidence intervals overlap slightly. Intrinsic absorption is strongly indicated in the SSS spectra, with $N_H = 7.9$(6.8–9.1) $\times 10^{20}$ cm^{-2}, which is ~ 9 times larger than the Galactic column in this line of sight.

3.4.2. *Joint Spectral Fits*

1. *Raymond-Smith Models.*—In joint spectral fits, the simplest reasonable model employing RS components is characterized by a single temperature, abundance, and absorbing column for both spectral data sets. This model did not provide a good fit, having $\chi^2_\nu = 1.31$ (see T5.3).

Having the SSS spectra characterized by a cooler temperature than the LAC spectrum motivated a joint, two-temperature fit to both data sets. As before, the cooler

component was assumed to be completely contained within the SSS field of view, so it had the same normalization for both the SSS and LAC spectra. With the abundances of the two temperature components tied together, the resulting best fit is shown in Figure 9 and has $\chi^2_\nu = 1.15$ for $\nu = 271$ (see T5.4). The higher temperature component, with $kT = 5.28$ (4.86–5.46) keV, is ~20% hotter than indicated by the LAC spectrum alone. The temperature of the cooler component, $kT = 3.15$ (1.82–3.36) keV, is consistent with the temperature found in the isothermal analysis of the SSS spectra alone (see T5.2). The χ^2 distributions for the two temperature components are shown in Figure 2*d*, while that of the (tied) abundance is in Figure 3*d*. The intrinsic absorption has the same large column that was found in the previous SSS analysis, $N_H = 8.1(7.1–24.7) \times 10^{20}$ cm^{-2}, and its χ^2 distributions is shown in Figure 4*d*. The ratio of model fluxes in the SSS and LAC fields of view is consistent with that derived from IPC imaging data. When we allowed the fractional abundances of the two temperature components to vary independently, the fit was not significantly improved and the best-fit abundance of the cool component was only ~25% higher than that of the hot component—their 90% comfidence limits also overlapped substantially. Isothermal models with either one or two abundances provided much worse fits. A variable covering fraction model for the intrinsic absorption had a best-fit value of unity for the covering fraction, with a 90% confidence lower limit of 73%.

A better fit was provided by a two-temperature model with a single global absorption component (see T5.5), rather than the combination of fixed Galactic N_H plus variable intrinsic absorption described above. However, the SSS/LAC flux ratio in this model *exceeds* that derived from IPC imaging data (by 5%), so this model is not preferred: since the LAC field of view exceeds that of the IPC, the SSS/LAC model flux ratio should be less than or equal to that derived from the IPC.

To assess whether the central component spreads significantly outside the SSS field of view, we allowed the cool component normalization to vary independently in the SSS and LAC spectral groups: the best-fit values did not differ significantly. We also added a third RS component which was allowed to be seen by the LAC alone, and this also failed to significantly improve χ^2. The amount of flux this third (cool) component ended up contributing to the LAC passband was ~1%. This is at the level expected from uncertainties in calibration and unresolved background sources.

2. *Cooling flow models.*—As previously, we assessed the model-dependence of the abundance and intrinsic N_H estimates by considering a spectral model incorporating a cooling flow component. The cooling flow was again assumed to be isobaric, with an initial temperature equal to that of the exterior isothermal atmosphere, and the cooling flow normalization (accretion rate) was the same for the SSS and LAC spectra. This cooling flow model provided a better fit than any of the previous two-temperature models, having $\chi^2_\nu = 1.05$ for $\nu = 271$ (see T5.6). The best-fitting exterior temperature, $kT = 4.74$ (4.65–4.83) keV, is ~6% larger than that derived from the LAC spectrum alone. The abundances of the two spectral components were allowed to vary independently and the best-fitting cooling flow abundance was near cosmic, with $A_{cf} = 1.15$ (0.65–2.11) while the exterior gas had $A_{hot} = 0.37$ (0.30–0.43), somewhat smaller than that derived from the two-temperature fits (see Fig. 6*d* for its χ^2 distribution). The best-fitting intrinsic absorption column, $N_H = 3.0(2.7–3.4) \times 10^{21}$ cm^{-2}, is ~4 times larger than that associated with the previous two-temperature model. This is also twice as high as the value found by WFJMA. The accretion rate associated with the cooling flow is $\dot{M} = 150$ (129–173) $M_\odot$ yr^{-1}. The ratio of model fluxes in the SSS and LAC fields of view is consistent with that derived from IPC imaging data. The quality of this fit suggests that the bulk of the cooling flow emission is indeed within the SSS field of view. When the cooling flow normalizations were allowed to vary independently in the LAC and SSS data sets (to test whether there is significant cooling flow emission outside the SSS field of view) we found the normalizations did not differ significantly and the χ^2 was not signifi-

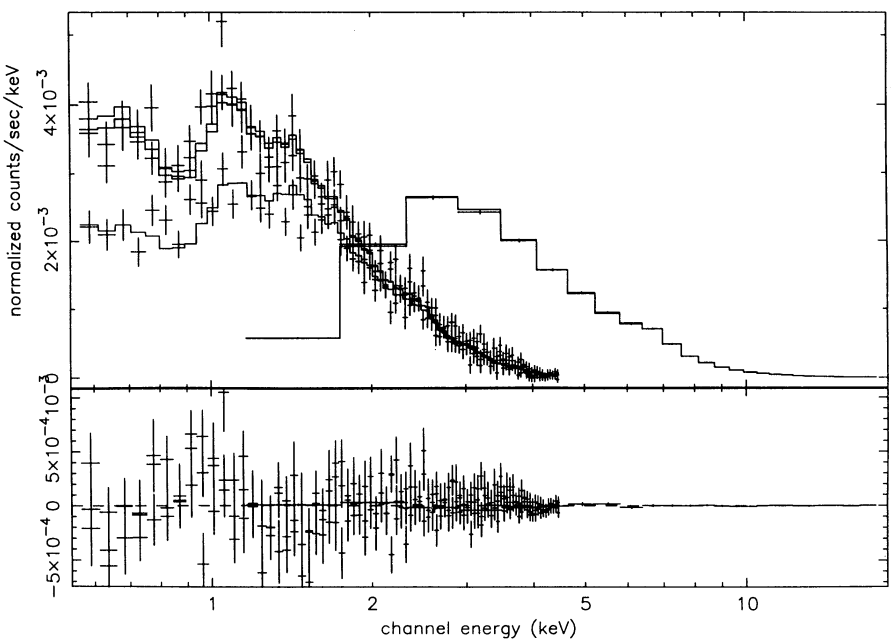

FIG. 9.—Two-temperature RS spectral models jointly fit to *Einstein* SSS and *Ginga* LAC data for A2199; see line 4 of Table 5 for best-fit parameters

cantly improved. To test the reality of the enhanced cooling flow abundances, we tied the abundances of the two spectral components together. The resulting best fit was significantly worse, having $\Delta\chi^2 = +7$ for $\Delta\nu = +1$ (for $\nu = 272$; see T5.7). The F-test shows that the need for the additional abundance component in the previous model (T5.6) is significant at the 99% level. A model allowing a partial covering fraction for the intrinsic absorption (but like the model in T5.6 in other respects) produced a best-fit value of unity for the covering fraction, with a 90% lower limit of greater than 85% coverage.

To test whether the intrinsic absorption component is truly intrinsic, we fitted a model with a single, variable, global absorption component. The resulting best-fit model (see T5.8) had $\Delta\chi^2 = +10$ compared to the previous best-fitting model, and the absorption was still ~ 9 times larger than the Galactic value, which is unlikely to be wrong by such a large factor. This poorer fit suggests that the intrinsic absorption is not globally distributed, but mostly confined within the SSS field of view.

We conclude that there is strong evidence for a cool emission component with intrinsic absorption in A2199. Evidence for an abundance gradient is model dependent: the dual RS models did not have compelling evidence for an abundance gradient, but the better fitting models with cooling flow spectra did have cooling flow abundances significantly enhanced compared to exterior gas.

4. SUMMARY AND DISCUSSION

We jointly analyzed *Ginga* LAC and *Einstein* SSS spectra for four galaxy clusters thought to contain cooling flows. Each cluster's spectra showed strong evidence for a relatively cool spectral component associated with the central cooling flow. The inclusion of these cool components caused the temperatures derived for the more dominant hotter components to be as much as $\sim 20\%$ larger than those derived from isothermal analyses, with $\sim 10\%$ increases being more typical. We found no compelling evidence for significant amounts of cool emission outside the central regions encompassed by the SSS field of view (i.e., within a 3′ radius of the center). We also explored the model-dependence in the amount of cool X-ray absorbing matter in each of the clusters; this cool absorbing material was first discovered by WFJMA to be ubiquitous in cooling flow clusters.

All four clusters show evidence of centrally enhanced metal abundances, with varying degrees of model dependence and statistical significance: the evidence is statistically strongest for A496 and A2142, weaker for A2199 and weakest for A1795. In A496, both dual-temperature RS spectral models and models incorporating cooling flow spectra provide the best fits when abundances are enhanced within the SSS field of view (at F-test confidence levels of 99.85% or greater when compared to a single-abundance model). Central abundance enhancement is also seen in both kinds of spectral models for A2142 (at F-test confidence levels of $\geq 99\%$ when compared to a single abundance model). In A2199, dual-temperature RS models see no significant central abundance enhancement, while the better-fitting cooling flow models do produce central abundance enhancements (the latter at an F-test significance level of 99% compared to a single-abundance model). Dual-temperature RS models for A1795 also showed no compelling evidence for a significant abundance gradient, but these models provided better overall fits than did models incorporating cooling flows, which did show evidence of a central abundance gradient (at an F-test confidence level of 95% relative to a single abundance model).

Previous observations of abundance distributions in clusters have also produced rather disparate results. In M87/Virgo, Lea et al. (1982) used two pointings of the *Einstein* SSS to determine that abundances were about solar at the center and stayed so out to 7′ from the center. However, Koyama et al. (1991) found the abundance to drop from ~ 0.5 solar at the center to only 0.1–0.2 solar beyond 1° from the center in a scanning observation with the *Ginga* LAC.

Ulmer et al. (1987) found in a *Spartan 1* observation of the Perseus cluster (A426) that the iron abundance dropped from 0.8 solar within 5′ to 0.4 solar between 6′ and 20′ from the center. A recent reanalysis of the *Spartan 1* data finds a somewhat steeper abundance gradient (Kowalski et al. 1993). Ponman et al. (1990) claim an even steeper abundance gradient in *Spacelab 2* spectra of Perseus, with iron practically vanishing beyond $\sim 20'$. Meanwhile, Edge (1990) found no abundance gradient within $\sim 20'$ in *EXOSAT* data. Recent *BBXRT* results by Arnaud et al. (1993) show no abundance gradient out to 13′, but the measured abundances are greater than those indicated by the previously noted spectra from broad-beam instruments.

For the Coma cluster (A1656), Hughes et al. (1988) and Edge (1990) used several *EXOSAT* pointings to deduce that the iron abundance is roughly constant out to 45′. More recently, Hughes et al. (1993) used a combination of *Tenma*, *EXOSAT*, and *Ginga* data to limit the allowed spatial distribution of iron in the Coma cluster. These authors found that any gradient in the iron distribution must be shallow and that, in fact the total mass of iron in the cluster out to 2 Mpc can be no less than $\sim 75\%$ of the amount estimated assuming a uniform iron distribution.

In *BBXRT* observations of NGC 1399, the central galaxy in the Fornax cluster, Serlemitsos et al. (1993) found roughly half-solar abundances out to $\sim 8'$, with weak evidence for an outward decline. A spatially unresolved *Ginga* LAC spectrum of this object indicates somewhat higher, nearly solar abundances (Ikebe et al. 1992).

In a continuation of this diverse theme, recent metallicity determinations from *ROSAT* PSPC observations of gas in groups of galaxies have also produced varying results with regard to overall abundances: Ponman & Bertram (1993) found a very low metal abundance ($\sim 15\%$ solar) in the compact group HCG 62. Mulchaey et al. (1993) also found abundances to be small ($\lesssim 20\%$ solar) in the NGC 2300 group. However, David, Forman, & Jones (1994) found abundances of $\sim 80\%$ solar in the NGC 5044 group, with no discernible gradient. The low metallicities in the HCG 62 and NGC 2300 groups are in conflict with the metallicity-temperature trend found in rich clusters, where cool clusters have higher abundances than hot clusters do (Hatsukade 1989; Edge & Stewart 1991).

Summarizing these disparate observations, some clusters seem to have fairly flat abundance distributions in their inner regions, while others have centrally enhanced abundances, and some may have declining abundances in their outskirts. Early results on abundances in groups show a large scatter, and represent a significant departure from the metallicity-temperature anticorrelation observed in rich clusters.

These observations raise the question: why are abundances centrally enhanced in some clusters, but not in others? In addressing this issue we need to consider the dominant

mechanism(s) by which intracluster metals are injected into intracluster gas in the first place. The two mechanisms proposed most often for metal contamination in intracluster gas are supernovae-driven protogalactic winds (Larson & Dinerstein 1975, Vigroux 1977; De Young 1978) and ram-pressure stripping of gas from galaxies (Gunn & Gott 1972; Norman & Silk 1979; Sarazin 1979; Nepveu 1981). Whereas protogalactic winds would inject both metals and energy into intracluster gas, ram-pressure stripping would inject only metals (White 1991). Current observations of X-ray surface brightness profiles and spectra of intercluster gas indicate that the gas seems to have a greater specific energy than cluster galaxies, with the disparity being largest for cool clusters (White 1991). This suggests the gas has experienced energy deposition in excess of that associated with cluster collapse, which is indicative of protogalactic winds (David et al. 1990; White 1991). Spatially resolved spectra for many clusters are required to confirm whether intracluster gas, particularly in cool clusters, has significantly more specific energy than cluster galaxies.

Observations of the metallicity of distant clusters may also constrain the source of metals. The detection of metals in very distant clusters would suggest a protogalactic wind origin. If the metals are primarily due to gas ram-pressure stripped from galaxies, the metallicity may build more slowly and secularly, as the central gas density of the cluster increases over time and supplements galaxy-galaxy stripping encounters.

If galactic winds are necessary to account for some of the energy content of intracluster gas, one may expect that the metals borne by the winds would be well mixed in the cluster. This may account for the bulk of the metals in the intracluster gas, but makes the central abundance enhancement in some clusters problematic.

There are several possible causes of the centrally enhanced abundances in some clusters, including: (1) in the context of the galactic wind origin for metals, a population gradient of wind-blowing galaxies in the cluster may imprint an abundance gradient; that is, if only early-type galaxies had winds, the fact that the fraction of early-type galaxies declines outward in a cluster may lead to a declining metallicity gradient; (2) metal-rich gas may be preferentially stripped from galaxies passing through the dense gas at cluster centers (Nepveu 1981); (3) metal-rich stellar mass loss in a central dominant galaxy may accumulate within the galaxy if some fraction of the stellar ejecta does not participate in its cooling flow; (4) given that the central dominant galaxy in a cluster has the deepest potential well of any galaxy in the cluster, the metals ejected by its protogalactic wind (if it had one) may not escape or be well mixed, remaining confined mostly near the cluster center; (5) given the anticorrelation of metallicity and temperature in intracluster gas, perhaps clusters with central abundance enhancements have ingested a relatively cool, metal-rich subcluster; (6) heavy ions may have gravitationally settled from exterior parts of the cluster (Fabian & Pringle 1977); however, it is now thought that the timescale for ionic settling to occur is too long for it to be important (Raphaeli 1978).

The first possibility above, that abundance gradients may be imprinted by population gradients in wind-blowing galaxies, can be tested by comparing observed population gradients with the many intracluster abundance profiles that will be derived in the near future from *ASCA* satellite data. Clusters without metallicity gradients in the inner regions may have particularly low spiral fractions, so any population gradient would be weak in the inner regions. The Coma and Perseus clusters are consistent with this. A2142 provides a possible counterexample, since it is a very hot cluster, so it is likely to have a small spiral fraction, but the analysis of this paper suggests it has a substantial central abundance enhancement. Another problem with this hypothesis is that the observed temperature-metallicity anticorrelation for clusters may provide counterevidence, since cool clusters tend to have smaller fractions of early-type galaxies, but have the highest metal abundances.

The second possibility, that galaxies are preferentially ram-pressure stripped in cluster centers, also has some difficulties: the metallicity of the gas stripped from galaxies must be at least equal to that of the central regions, which may be near solar. However, if spiral galaxies are the primary source of stripped gas, the gas will come largely from the outer parts, where the average metallicity in extended H I disks is likely to be less than solar. Furthermore, if the metal-rich gas is largely stripped from early-type galaxies, their abundances are turning out to be very subsolar: for example, *BBXRT* observations of NGC 4472 in the Virgo cluster reveal an iron abundance of ~ 0.2 solar (Serlemitsos et al. 1993). This process is unlikely to produce strong gradients in the cores of rich clusters like Coma, since the stripping saturates (Hughes et al. 1993).

The third and fourth possibilities listed above attribute central abundance enhancements to the stellar mass loss of the central dominant galaxies. Even if the central abundances were not 2–3 times greater than the exterior or average abundances, the total amount of metals is about two orders of magnitude too large to be generated by current stellar mass-loss rates in the central dominant galaxies; however, it is possible that the metals had accumulated in the vicinity for a long time, due to protogalactic winds from or atmospheric stripping of the central dominant galaxy and neighboring galaxies in the core regions. The current cooling flows, which extend 100–200 kpc from the cluster centers, will then consist of this particularly metal rich gas. The historical contribution of the central dominant galaxies' mass loss may be assessed by determining the physical extent of the abundance-enhanced region.

The fifth possibility mentioned above is that a cool, high-metallicity subcluster may merge with and settle to the center of a hotter, lower metallicity cluster to create a central abundance enhancement. One may then expect some correlation between the existence of central abundance enhancements and signs of a merger. A496 and A1795 provide counterexamples to this expectation: A496 appears to have centrally enhanced abundances but has no signs of a significant recent merger; A1795 has only weak evidence of centrally enhanced abundances, but the high peculiar velocity of its central cD is suggestive of a recent merger. Alternatively, cluster mergers may act in the opposite sense, by washing out preexisting metallicity gradients, particularly if the subclumps are of comparable mass, so the gravitational potential is maximally perturbed. A recent numerical simulation by Roettiger, Burns, & Loken (1993) suggests that the *dark matter* component of subclump material will be thoroughly mixed during the merger, but the mixture of the *gas* was not discussed. A more recent simulation by Pearce, Thomas, & Couchman (1994) suggests that gas in cluster cores does not mix completely during mergers. This lack of complete gas mixing is supported by a recent *BBXRT* observation of the merging cluster A2256, which suggests that a preexisting cooling flow in one of the two major subclumps has been disrupted, but a region of relatively cool, X-ray absorbing gas still persists (Miyaji et al. 1993); the merging

system is not yet relaxed, so it is not clear whether this possible cooling flow remnant will retain its coherence postrelaxation. If mergers homogenize at least the central abundance distributions, then one expects an anticorrelation between the existence of central abundance enhancements and signs of significant mergers. At present, this seems more consistent with the observations: A496 and Virgo are examples of clusters with central abundance enhancements but no evidence of a recent disruptive merger, while Perseus and Coma are clusters with centrally homogeneous metal distributions and evidence of significant mergers (if the binary central dominant galaxies in Coma can be interpreted as relics of two former subclusters). A1795 may be added to the latter list if the weakness of its evidence for a central abundance enhancement is emphasized. Counterexamples to this trend may be provided by A2142 and A2199, which seem to have centrally enhanced abundances but also have signs of significant mergers (if binary central dominant galaxies are again taken to be such a sign in the case of A2142).

Spatially resolved spectra from the *ASCA* satellite will be able to provide more accurate assessments of abundance gradients in intracluster gas. As *ASCA* spectra accumulate for many clusters, the energetics of the gas can be compared to those of the galaxies and the dark matter to determine whether protogalactic winds are indicated. The overall metallicity and the nature of any metallicity gradients will be more readily correlated with other cluster properties, such as spiral fraction, in order to determine whether the primary metal injection mechanism is galactic winds or ram-pressure stripping. Finally, correlating the presence or absence of central abundance enhancements with such cluster properties as the local spiral fraction or merger signatures will help determine whether a separate metal injection mechanism is required to create them.

R. E. W., C. S. R. D., and J. P. H. thank F. Makino and the Institute of Space and Astronautical Science for their hospitality and scientific support during our stays in Japan. We also thank K. Arnaud, A. Tennant, and O. Day for invaluable help with XSPEC, and R. Mushotzky for stimulating discussions. We especially appreciate the effort by K. Arnaud, R. Johnstone, and D. White in developing the cooling flow model within XSPEC. J. P. H. thanks M. Arnaud and K. Yamashita for advice and assistance during the preliminary reduction of the A2199 *Ginga* LAC data. We thank the referee, P. Thomas, for helpful suggestions. R. E. W. and C. S. R. D. were supported in part by NASA grant NAG 8-228. Additional support for R. E. W. was provided by the NSF and the State of Alabama via EPSCoR II. J. P. H. was supported in part by NASA grant NAG 8-181. This research has made use of data obtained through the High Energy Astrophysics Science Archive Research Center On-line Service, provided by the NASA-Goddard Space Flight Center. This research has also made use of the NASA/IPAC Extragalactic Database (NED), which is operated by the Jet Propulsion Laboratory, Caltech, under contract with NASA.

REFERENCES

Allen, C. W. 1976, Astrophysical Quantities (Athlone: London)
Allen, S. W., Fabian, A. C., Johnstone, R. M., Nulsen, P. E. J., & Edge, A. C. 1992, MNRAS, 254, 51
Allen, S. W., Fabian, A. C., Johnstone, R. M., White, D. A., Daines, S. J., Edge, A. C., & Stewart, G. C. 1993, MNRAS, 262, 901
Arnaud, K. A., & Fabian, A. C. 1987, preprint
Arnaud, K. A., et al. 1993, preprint
Arnaud, M., Hughes, J. P., Forman, W., Jones, C., Lachieze-Rey, M., Yamashita, K., & Hatsukade, I. 1992, ApJ, 390, 345
Arnaud, M., Lachieze-Rey, M., Rothenflug, R., Yamashita, K., & Hatsukade, I. 1992, A&A, 243, 67
Birkinshaw, M., Hughes, J. P., & Arnaud, K. A. 1991, ApJ, 379, 466
Canizares, C. R., Markert, T. H., & Donahue, M. E. 1988, in Cooling Flows in Clusters and Galaxies, ed. A. C. Fabian (Dordrecht: Kluwer), 63
Christian, D. J., Swank, J. H., Szymkowiak, A. E., & White, N. E. 1992, Legacy, 1, 38
Cowie, L., Hu, E. M., Jenkins, E. B., & York, D. G. 1983, ApJ, 272, 29 (CHJY)
David, L. P., Arnaud, K. A., Forman, W., & Jones, C. 1990, ApJ, 356, 32
David, L. P., Forman, W., & Jones, C. 1994, preprint
Day, C. S. R., Fabian, A. C., Edge, A. C., & Raychaudhury, S. 1991, MNRAS, 252, 394
De Young, D. 1978, ApJ, 223, 47
Drake, S., Arnaud, K., & White, N. 1992, Legacy, 1, 43
Edge, A. C. 1990, Ph.D. thesis, Univ. of Leicester
Edge, A. C., & Stewart, G. C. 1991, MNRAS, 252, 414
Edge, A. C., Stewart, G. C., Fabian, A. C., & Arnaud, K. A. 1990, MNRAS, 245, 559
Elvis, M., Green, R. F., Bechtold, J., Schmidt, M., Neugebauer, G., Soifer, B. T., Matthews, K., & Fabbiano, G. 1986, ApJ, 310, 291
Fabian, A. C., & Pringle, J. E. 1977, MNRAS, 181, 5p
Gebhardt, K., & Beers, T. C. 1991, ApJ, 383, 72
Gunn, J. E., & Gott, J. R., III 1972, ApJ, 176, 1
Hatsukade, I. 1989, Ph.D. thesis, Osaka University
Heckman, T. M. 1981, ApJ, 250, L59
Hoessel, J. G. 1980, ApJ, 241, 493
Hughes, J. P., Butcher, J. A., Stewart, G. C., & Tanaka, Y. 1993, ApJ, 404, 611
Hughes, J. P., Gorenstein, P., & Fabricant, D. 1988, ApJ, 329, 82
Hughes, J. P., & Tanaka, Y. 1992, ApJ, 398, 62
Ikebe, Y., et al. 1992, ApJ, 384, L5
Johnstone, R. M., Fabian, A. C., Edge, A. C., & Thomas, P. A. 1992, MNRAS, 255, 431
Kowalski, M. P., Cruddace, R. G., Snyder, W. A., & Fritz, G. G. 1993, ApJ, 412, 489
Koyama, K., Takano, S., & Tawara, Y. 1991, Nature, 350, 135
Larson, R. B., & Dinerstein, H. L. 1975, PASP, 87, 911
Lea, S. M., Mushotzky, R. F., & Holt, S. S. 1982, ApJ, 262, 24
Makino, F., & Astro-C Team 1987, Ap. Lett. Comm., 25, 223
Masai, K. 1984, Ap&SS, 98, 367
McHardy, I. M., Stewart, G. C., Edge, A. C., Cook, B., Yamashita, K., & Hatsukade, I. 1990, MNRAS, 242, 215
McNamara, B. R., & O'Connell, R. W. 1992, ApJ, 393, 579
Miyaji, T., et al. 1993, ApJ, 419, 66
Morrison, R., & McCammon, D. 1983, ApJ, 270, 119
Mulchaey, J. S., Davis, D. S., Mushotzky, R. F., & Burnstein, D. 1993, ApJ, 404, L9
Mushotzky, R. F. 1984, Phys. Scripta, T7, 157
Mushotzky, R. F., & Szymkowiak, A. E. 1988, in Cooling Flows in Clusters and Galaxies, ed. A. C. Fabian (Dordrecht: Kluwer), 53
Nepveu, M. 1981, A&A, 101, 362
Norman, C., & Silk, J. 1979, ApJ, 233, L1
Nulsen, P. E. J., Stewart, G. C., Fabian, A. C., Mushotzky, R. F., Holt, S. S., Ku, W., H.-M., & Malin, D. F. 1982, MNRAS, 199, 1089
Pearce, F. R., Thomas, P. A., & Couchman, H. M. P. 1994, MNRAS, in press
Ponman, T. J., & Bertram, D. 1993, Nature, 363, 51
Ponman, T. J., et al. 1990, Nature, 347, 450
Raphaeli, Y. 1978, ApJ, 225, 335
Raymond, J. C., & Smith, B. W. 1977, ApJS, 35, 419
Reichert, G. A., Mason, K. O., Thorstensen, J. R., & Bowyer, S. 1982, ApJ, 260, 437
Roettiger, K., Burns, J., & Loken, C. 1993, ApJ, 407, L53
Sarazin, C. L. 1979, Astrophys. Lett., 20, 93
Serlemitsos, P. J., Loewenstein, M., Mushotzky, R. F., Marshall, F. E., & Petre, R. 1993, ApJ, 413, 518
Stark, A. A., Gammie, C. F., Wilson, R. W., Bally, J., Linke, R. A., Heiles, C., & Hurwitz, M. 1992, ApJS, 79, 77
Stewart, G. C., Fabian, A. C., Jones, C., & Forman, W. 1984, ApJ, 285, 1
Szymkowiak, A. E. 1986, Ph.D. thesis, Univ. of Maryland (NASA TM No. 86169)
Takano, S., Awaki, H., Koyama, K., Kunieda, H., Tawara, Y., Yamauchi, S., Makishima, K., & Ohashi, T. 1989, Nature, 340, 289
Thomas, P. A., Fabian, A. C., & Nulsen, P. E. J. 1987, MNRAS, 228, 973
Turner, M. J. L., et al. 1989, PASJ, 41, 373
Ulmer, M. P., et al. 1987, ApJ, 319, 118
Vigroux, L. 1977, A&A, 56, 473
Wang, Q., & Stocke, J. T. 1993, ApJ, 408, 71
White, D. A., Fabian, A. C., Johnstone, R. M., Mushotzky, R. F., & Arnaud, K. A. 1991, MNRAS, 252, 72 (WFJMA)
White, R. E., III. 1991, ApJ, 367, 69
White, R. E., III, & Sarazin, C. L. 1987, ApJ, 318, 621
Zabludoff, A. I., Huchra, J. P., & Geller, M. J. 1990, ApJS, 74, 1 (ZHG)